Repeated photodynamic therapy mediates the abscopal effect through multiple innate and adaptive immune responses with and without immune checkpoint therapy

Jenny Lou[1,2]*, Masato Aragaki[3,4,]*, Nicholas Bernards[3], Tess Chee[5], Alexander Gregor[3], Yoshihisa Hiraishi[3], Tsukasa Ishiwata[3], Chelsea Leung[4], Lili Ding[2], Shinsuke Kitazawa[3], Takamasa Koga[3], Yuki Sata[3], Hiroyuki Ogawa[3], Juan Chen[2], Tatsuya Kato[5], Kazuhiro Yasufuku[2,3], Gang Zheng[1,2]

1. Department of Medical Biophysics, University of Toronto, Toronto, Ontario M5G 1L7, Canada.
2. Princess Margaret Cancer Centre, University Health Network, Toronto, Ontario M5G 1L7, Canada.
3. Division of Thoracic Surgery, Toronto General Hospital, University Health Network, Toronto, Ontario M5G 2C4, Canada.
4. Institute of Biomedical Engineering, University of Toronto, Toronto, Ontario, M5S 3G9, Canada.
5. Department of Thoracic Surgery, Hokkaido University Faculty and School of Medicine, Sapporo, Hokkaido 060-8638, Japan.
6. Faculty of Health Sciences, McMaster University, Hamilton, Ontario L8S 4L8, Canada

Corresponding Authors:
Dr. Gang Zheng, (ORCID: 0000-0002-0705-7398) University of Toronto, PMCRT 5-354, 101 College Street, Toronto, ON, M5G 1L7, Canada, E-mail: gang.zheng@uhnres.utoronto.ca
Dr. Kazuhiro Yasufuku, (ORCID: 0000-0002-3053-4156) Toronto General Hospital, University Health Network, University of Toronto, 200 Elizabeth Street, EN 9N-957, Toronto, ON M5G 2C4, Canada. E-mail: Kazuhiro.Yasufuku@uhn.ca

***** Co-first authors.

Abstract

In combination with immune checkpoint inhibitors, photodynamic therapy can induce robust immune responses capable of preventing local tumor recurrence and delaying the growth of distant, untreated disease (ie. the abscopal effect). Previously, we found that repeated photodynamic therapy (R-PDT) using porphyrin lipoprotein (PLP) as a photosensitizer, without the addition of an immune checkpoint inhibitor, can induce the abscopal effect. To understand why PLP mediated R-PDT alone can induce the abscopal effect, and how the addition of an immune checkpoint inhibitor can further strengthen the abscopal effect, we investigated the broader immune mechanisms facilitated by R-PDT and combination R-PDT + anti-PD-1 monoclonal antibody (αPD-1) in a highly aggressive, subcutaneous AE17-OVA mesothelioma dual tumor-bearing C57BL/6 mice.

We found a 46.64-fold and 61.33-fold increase in interleukin-6 (IL-6) after R-PDT and combination R-PDT + αPD-1 relative to PBS respectively, suggesting broad innate immune activation. There was a greater propensity for antigen presentation in the spleen and distal, non-irradiated tumor draining lymph nodes, as dendritic cells and macrophages had increased expression of MHC class II, CD80, and CD86, after R-PDT and combination R-PDT + αPD-1. Concurrently, there was a shift in the proportions of CD4+ T cell subsets in the spleen, and an increase in the frequency of CD8+ T cells in the distal, non-irradiated tumor draining lymph

nodes. While R-PDT had an acceptable safety profile, combination R-PDT + αPD-1 induced 1.26-fold higher serum potassium and 1.33-fold phosphorus, suggestive of mild laboratory tumor lysis syndrome. Histology revealed an absence of gross inflammation in critical organs after R-PDT and combination R-PDT + αPD-1 relative to PBS-treated mice. Taken together, our findings shed light on how the abscopal effect can be induced by PDT and strengthened by combination R-PDT + αPD-1, and suggests minimal toxicities after R-PDT.

Keywords: photodynamic therapy, immune response, porphyrin, immunotherapy, thoracic malignant tumor, PD-1

Introduction

Photodynamic therapy (PDT) involves the delivery of a photosensitizer to a tumor and subsequent irradiation of the photosensitizer-laden tumor tissue. The activation of the photosensitizer generates reactive molecular species that can induce death of tumor cells through multiple mechanisms, including apoptosis, necrosis, autophagy, necroptosis, and immunogenic cell death [1–3]. PDT has been clinically approved to treat melanoma, bladder, esophageal, and non-small cell lung cancer [4].

While effective in eradicating irradiated tumors, PDT has also eliminated non-irradiated distant metastases, as reported in case studies[5]. This phenomenon is mediated through an immune response, termed the abscopal effect (refer to Figure 1). More commonly observed in radiotherapy, the abscopal effect consists of multiple steps: first, immunogenic cell death is induced, and dying cells release damage-associated molecular patterns (DAMPs) [1]. Second, antigen presenting cells (APCs) such as macrophages and dendritic cells are recruited to the tumor, where they phagocytose tumor antigens [3,6,7]. Third, there is an adaptive immune response involving T-cell priming by APCs[8]. Fourth, T cells migrate to the non-irradiated tumor and their effector actions can contribute to control and/or elimination of distant disease.

By itself, PDT is often unable to induce a robust abscopal effect. To initiate the abscopal effect, PDT is often combined with immune checkpoint inhibitors[9,10]. Combination PDT with anti-cytotoxic T-lymphocyte antigen 4 (CTLA-4) has been investigated to induce an abscopal effect in different tumor models, including in dual CT26 colorectal tumors in mice[11] and lung metastases in 4T1 breast tumor-bearing mice[12]. Others have employed combination PDT with anti-programmed death protein (PD-1) or anti-programmed death ligand 1 (PD-L1) inhibitors to eliminate tumors in various models, including non-irradiated 4T1 breast tumors[13,14], non-irradiated lung metastases in 4T1 breast tumor-bearing mice and distant tumors in TUBO breast tumor-bearing mice[15], and lung metastases in B16F10 melanoma tumor-bearing mice[16]. Meanwhile, triple combination therapy consisting of PDT, anti-PD-L1, and oxaliplatin has been used to induce the abscopal effect in mice bearing CT26 colorectal tumors[17].

In our lab, we previously developed a novel theranostic photosensitizer, porphyrin lipoprotein (PLP)[18]. PLP is a ~20 nm, multimodal biomimetic nanoparticle that can serve as a photosensitizer, fluorophore, and PET imaging agent, upon chelation with Cu-64. After administering PDT with PLP four times repeatedly, we observed an abscopal effect in C57/BL6 mice bearing dual, subcutaneous AE17-OVA mesotheliomas[19]. When PDT was performed four times, termed repeated PDT (R-PDT), irradiated tumors were eradicated while non-irradiated tumors had a delay in tumor growth. Two weeks after the initial injection of PLP, mice that received R-PDT had a 4.2-fold and 4.1-fold smaller non-irradiated tumor volume, compared to laser control or PLP only treated mice respectively (Figure 2, panel A).

Programmed cell death protein 1 (PD-1) is an inhibitory receptor expressed on activated T cells. By blocking the interaction of PD-1 receptors with PD-L1 expressed on tumor cells, or tumor microenvironment macrophages, anti-PD-1 antibodies (∝PD-1) can reverse exhaustion of activated T cells[20]. ∝PD-1 are clinically approved for the treatment of various cancers, including

melanoma, non-small cell lung cancer, colorectal cancer, gastric cancer, and malignant pleural mesothelioma[21]. Previously, we found the addition of ∝PD-1 to R-PDT further delayed non-irradiated tumor growth and improved survival relative to R-PDT or ∝PD-1 therapy alone (Figure 2, panel B)[19].

To follow-up and improve our understanding of how monotherapy PDT can induce the abscopal effect, we systemically investigated the immune mechanisms underlying the abscopal effect after R-PDT. While many studies investigate the anti-tumoral efficacy of combination therapy, there are few that explore in-depth the immune responses underlying combination therapy. Therefore, we also investigated the broader immune responses potentiated by combination R-PDT + ∝PD-1, relative to monotherapy R-PDT or ∝PD-1 (Figure 2, panel C). By evaluating immune populations in the distal, non-irradiated tumor, spleen, and non-irradiated tumor draining lymph nodes, as well as serum cytokines, we hope to establish a broader understanding as to how R-PDT and combination R-PDT + ∝PD-1 can induce the abscopal effect. Then, to determine whether greater immune activation induces toxicities, we assessed the safety of R-PDT and combination R-PDT + ∝PD-1. Taken together, this knowledge can be leveraged to strengthen immune responses after PDT or combination therapy to elicit durable, systemic, and safe anti-tumor responses.

After R-PDT and combination R-PDT + ∝PD-1, we observed many changes in immune cell populations across the distal, non-irradiated tumor, spleen, and non-irradiated tumor draining lymph node, as well as changes in serum cytokines. There was evidence of innate immune system activation via increases in serum IL-6. Increased maturation of APCs and expression of downstream costimulatory markers, in both the spleen and non-irradiated tumor draining lymph nodes, were noted, with subsequent shifts in the frequencies of splenic and non-irradiated tumor draining lymph node T cell subsets. Despite the systemic immune activation, we did not observe greater CD4 or CD8+ T cell infiltration across multiple organs, relative to saline-treated mice. Moreover, organ architecture was preserved across multiple organs. Combination R-PDT + ∝PD-1 induced increases in potassium and phosphorus that is consistent with laboratory tumor cell lysis syndrome. Accordingly, the reasonable safety profile of R-PDT shows potential for clinical translation.

Methods

Materials

To formulate PLP nanoparticles, the following lipids were obtained from Avanti Polar Lipids: 1, 2-dimyristoyl-sn-glycero-3-phosphocholine (DMPC) and cholesteryl oleate. Porphyrinlipid was synthesized in-house. 0.1 μm membrane filters for nanoparticle filtration were obtained from Millex®, Sigma-Aldrich. Cells were cultured in Roswell Park Media 1640 (RPMI-1640), fetal bovine serum (FBS) and penicillin/streptomycin from Gibco. Phosphate buffered saline (PBS) was procured from Gibco. For treatment of mice, α-PD-1 antibodies were purchased from BioXCell (clone RMP-14).

For flow cytometry experiments, the following antibodies were purchased from BioLegend: PE anti-mouse CD3ε antibody (clone 145-2C11), PerCP/Cyanine5.5 anti-mouse CD4 antibody (clone RM4-5), APC/Cy7 anti-mouse CD8a antibody (clone 53-6.7), and BV 510 anti-mouse

CD62L antibody (clone MEL-14), TruStain FcX™ anti-mouse CD16/32, PE F4/80 (clone BM8), Brilliant Violet MHC IA/IE (clone M5/114.15.2), FITC CD80 (clone 16-10A1), Brilliant Violet 421 CD86 (clone GL-1), APC/Cy7 CD11b (clone M1/70), Brilliant Violet 605 NK1.1 (clone PK136), and PE/Cy7 CD11c (clone N418), PE/Cy7 CD25 (clone PC61), BV605 anti-mouse CD44 (clone IM7). For tumor digestion in the flow cytometry experiments, collagenase IV and DNAse I were purchased from Sigma Aldrich and Thermo Scientific.

Porphyrin lipoprotein synthesis

Formulation of PLP was completed, as per the methods outlined by Cui et al[18]. First, a lipid film comprised of 0.9 µmol porphyrin-lipid, 2.1 µmol DMPC, and 0.3 µmol cholesteryl oleate, was synthesized via dissolution of lipids in chloroform and drying by nitrogen. Next, the film was hydrated with PBS and bath sonicated for 1 h. After, R4F peptide (2.3 mg; 5 mg/mL) was incorporated to the nanoparticle solution drop-wise until the turbid solution became transparent. The next day, the solution was centrifuged at 12 000 rpm for 5 minutes.

Briefly, a lipid film consisting of 0.9 µmol porphyrin-lipid, 2.1 µmol DMPC, and 0.3 µmol cholesteryl oleate was formed. The film was subsequently hydrated with PBS (150 mM, pH 7.5) and bath sonicated for 1 h. R4F peptide (2.3 mg; 5 mg/mL) was added dropwise to the solution, after which the turbid solution became transparent. The next day, the solution was centrifuged at 12 000 rpm for 20 minutes, and the supernatant was filtered through a 0.1 µm membrane (Millex®, Sigma-Aldrich).

Cell culture

AE17-OVA+ mesothelioma cells were gifted by Dr. Marc de Perrot (University of Toronto, Toronto, Ontario, Canada). AE17-OVA+ cells were cultured at 37ºC in 5% CO_2 in RPMI-1640 media, supplemented with FBS (5% v/v), 100 U/mL penicillin, 100 mg/mL streptomycin and nonessential amino acids.

In vivo testing

All in vivo animal experiments were approved by the University Health Network Animal Care Committee (AUP#4151). Experiments adhered with all relevant institutional, provincial, and federal requirements.

Dual, subcutaneous AE17-OVA+ mesothelioma tumor model

One day prior to tumor inoculation, immunocompetent female C57BL/6 mice were anesthetized with isoflurane, and the hair on the hindlimbs were shaved. Then, hair removal cream (Nair) was applied to the hindlimb for ~10 minutes and cleansed. The next day, mice were inoculated with subcutaneous AE17-OVA tumors on both hindlimbs. Mice were anesthetized using isoflurane (5% induction, 2.5% maintenance). With a 25-gauge needle, mice were subcutaneously inoculated with $1x10^6$ AE17-OVA+ mouse mesothelioma tumor cells re-suspended in PBS, into both dorsal hindlimbs.

Treatments

Mice were randomly assigned to be treated with either: PBS, ∝PD-1, R-PDT, or combination R-PDT + ∝-PD-1. We defined the day of the first PLP, PBS, and/or ∝PD-1 antibody injection as "day 0". A schematic of the treatment schedule is shown in Figure 2, panel C. For PBS treatment, mice were intravenously injected with PBS on days 0, 3, 6, or 9. For ∝PD-1 treatment, mice were intraperitoneally injected with ∝PD-1 (12 mg/kg) on days 0, 3, 6, or 9.

For R-PDT treatment, mice were intravenously administered PLP injections on days 0, 3, 6, or 9. At 24 h post injection, the left tumors of mice were irradiated on days 1, 4, 7, and 10. For combination R-PDT + ∝ PD-1 treatment, mice were injected intravenously with PLP and intraperitoneally with ∝PD-1 four times in total (days 0, 3, 6, and 9), followed by laser irradiation (days 1, 4, 8, and 10). Mice treated with R-PDT or combination R-PDT + ∝PD-1 received light irradiation (671 nm wavelength, 100 mW/cm^2) for 5 minutes, at 24 h post-injection of PLP. Mice were sacrificed on day 11 for flow cytometry and histology.

Flow Cytometry

On day 11, mice across all treatment groups were anesthetized with isoflurane and sacrificed via terminal cardiac puncture. Non-irradiated tumors, non-irradiated tumor draining lymph nodes, and the spleen were removed from each mouse for flow cytometry.

To digest tumors into single cell suspensions, tumors were minced and digested in collagenase IV and DNAse I in 37^{o}C for 30 minutes, while shaken on a MultiTherm (ThermoFisher). To stop the enzymatic reaction, EDTA (5 µM) was added. Subsequently, tumor cells were washed, centrifuged, and filtered.

For the digestion of non-irradiated tumor draining lymph nodes, mechanical digestion was employed. Lymph node cells were filtered through a 100 µm cell strainer (Falcon), washed with PBS, and centrifuged.

For processing of spleens into single cell suspensions, mechanical digestion was used. After filtration through a 100 µm cell strainer (Falcon), spleen samples were resuspended in erythrolysis buffer for 10 minutes. Following red blood cell lysis, samples were washed with PBS, centrifuged, and counted.

Cells were counted using a Vi-CELL XR Cell Viability Analyzer (Beckman Coulter). Then, spleen, lymph node, and tumor cells were split and incubated with TruStain FcX™ (1:50 dilution) for 20 minutes at 4^{o}C to block non-specific Fc receptor binding. After washing, centrifugation, and removal of supernatant, cells were stained with one of two antibody panels for 20 minutes at 4^{o}C. The first antibody panel comprised of PE CD3, PerCP/Cy5.5 CD4, APC/Cy7 CD8, Brilliant Violet 605 CD44, Brilliant Violet 510 CD62L, PE/Cy7 CD25, FITC CD127, and DAPI (BioLegend). The second panel consisted of PE F4/80, Brilliant Violet MHC IA/IE, FITC CD80, Brilliant Violet 421 CD86, APC/Cy7 CD11b, Brilliant Violet 605 NK1.1 and PE/Cy7 CD11c. Following antibody staining, samples were washed, centrifuged and stained with DAPI. Subsequently, samples were analyzed cytoFLEX S (Beckman Coulter, USA) and data were analyzed with FlowJo (TreeStar).

Serum analysis

On day 11, terminal cardiac puncture was performed using a 25-gauge needle inserted into the ventricles of the heart, with ~500 µL of blood obtained per mouse. Blood was rested at room

temperature for ~45 minutes to ensure clotting. Next, samples were centrifuged at 1000 g for 10 minutes, and the supernatant (ie. the serum) was collected for analysis. Half the serum was diluted in PBS two-fold and iced prior to shipment to Eve Technologies (Calgary, Canada) for serum analysis via the mouse pro-inflammatory focused 18-plex cytokine array. Multiplexing of granulocyte-macrophage colony-stimulating factor (GM-CSF), interferon-gamma (IFNγ), interleukin-1 beta (IL-1B), interleukin-2 (IL-2), interleukin-4 (IL-4), interleukin-5 (IL-5), interleukin-6 (IL-6), interleukin-7 (IL-7), interleukin-10 (IL-10), interleukin-12p70 (IL-12p70), interleukin-13 (IL-13), interleukin-17A (IL-17A), monocyte chemoattractant protein-1 (MCP-1), keratinocytes-derived chemokine (KC), and macrophage inflammatory protein-2 (MIP-2) and tumor necrosis factor alpha (TNF-∝) was conducted.

The remainder of the serum was submitted to the University Health Network's Animal Resource Centre for biochemical analysis via the VetScan VS2 (Zoetis). Total bilirubin, alanine aminotransferase, alkaline phosphatase, blood urea nitrogen, creatinine, potassium, calcium, sodium, phosphorus, glucose, and amylase were analyzed.

Histology

On day 11, mice were sacrificed and dissected to collect the brain, liver, lung, heart, kidney, liver, spleen, lymph nodes, irradiated and non-irradiated tumors for histology. All organs were fixed in 10% formalin for 3 days, and subsequently transferred to 70% ethanol. Next, samples were submitted to the STTARR Histopathology Core services for paraffin embedding, slicing, and staining of CD4 and CD8. Following this step, whole slide scanning at 20x magnification was performed (Aperio Scanscope XT whole-slide scanner, Leica Biosystems) at the Advanced Optical Microscopy Facility. Then, whole slide analysis of CD4 and CD8 staining across tissues was completed with Halo software using the cytonuclear analysis module.

Statistical Analyses

Statistical analysis was performed using GraphPad Prism version 8.4.3 for Macintosh (GraphPad Software, San Diego, California, USA, www.graphpad.com). For flow cytometry, serum cytokine, and Halo quantified histology data, we employed ordinary one-way ANOVAs and post-hoc Tukey's multiple comparisons tests to assess for significant differences in immune cell populations. Significance was set at $p<0.05$. Values are presented as mean ± standard deviation.

Results

1. **Repeated PDT alone and in combination with ∝PD-1induces an innate immune response**

Previously, we found that PLP mediated R-PDT induced the abscopal effect in a highly aggressive, dual subcutaneous AE17-OVA mesothelioma model in C57BL/6 mice. Mice treated with four cycles of PDT (R-PDT) had four-fold reduced growth on the distal, non-irradiated tumor, relative to controls (Figure 2, panel A)[19]. Moreover, R-PDT in combination with ∝PD-1 had prolonged survival, relative to mice treated PBS, R-PDT, and ∝PD-1 (Figure 2, panel B). As such, we aimed to determine the immune mechanisms underlying this abscopal effect.

After mice were treated with either PBS, ∝PD-1, R-PDT, or R-PDT + ∝PD-1, we evaluated their serum cytokine and chemokine levels. IL-6 is a pleiotropic cytokine secreted by various cells, including macrophages, B and T cells, and monocytes[22], and is involved in the stimulation of acute phase reactions, antibody production, and T-cell proliferation[23]. IL-6 was significantly greater after R-PDT, than after PBS and anti-PD-1 treated mice (Figure 3, panel A). Likewise, we observed a significantly greater increase in serum IL-6 for mice treated with R-PDT + ∝PD-1. Concurrently, mice treated with R-PDT, or R-PDT + ∝PD-1, compared to PBS or ∝PD-1, had reduced serum albumin (Figure 3, panel B). Associated with inflammation, the reduction of albumin may arise from IL-6, which can inhibit albumin synthesis in the liver[23]. There was a 2-fold elevation in serum globulins following both R-PDT and combination R-PDT + ∝PD-1 treatment over the other groups (Figure 3, panel C). Accordingly, this rise in the level of globulins suggests activation of B-cells and subsequent secretion of antibodies.

Neutrophils are the first responder lymphocytes to sites of injury and inflammation and can undergo effector functions such as oxidative burst or formation of neutrophil extracellular traps to defend against pathogens[24]. After R-PDT, we observed a decrease in serum chemokines responsible for neutrophil recruitment. Interleukin-1∝ (IL-1∝) is a pro-inflammatory cytokine that can serve as an alarmin and subsequently recruit neutrophils to the site of injury[25,26]. Mice treated with R-PDT and combination R-PDT + ∝PD-1 had 2.0- and 2.8-fold decreases in IL-1∝ relative to PBS treated mice (Figure 3, panel D). CXCL5 is a potent neutrophil chemoattractant and activator and has been associated with poor prognosis in patients with various types in cancers[27,28]. Serum levels of CXCL5 were decreased 2.4- and 2.9-fold in R-PDT and combination R-PDT + ∝PD-1, respectively (Figure 3, panel E). Macrophage inflammatory protein-2 (MIP-2), also known as CXCL2, is a potent chemoattractant produced by neutrophils[24]; Gollnick et al. previously demonstrated that neutrophil recruitment induced by PDT is dependent on the presence of MIP-2[29]. MIP-2 was also reduced for R-PDT and combination R-PDT + ∝PD-1 treated mice, relative to ∝PD-1 controls (Figure 3, panel F). Compared to PBS treated mice, combination R-PDT + ∝PD-1 treated mice had reduced MIP-2. Taken together, the reduction in serum IL-1∝, CXCL5, and MIP-2 suggests reduced neutrophil migration after R-PDT or combination R-PDT + ∝PD-1. Levels of other cytokines and chemokines in the serum were quantified and are reported in Supplementary Figures 1 and 2, respectively. No differences were observed between treatment groups for the following cytokines: GM-CSF, IFN-γ, IL-1β, IL-2, IL-4, IL-5, IL-7, IL-10, IL-12p70, IL-13, IL-17A, and TNF-α. Likewise, there were no differences in serum levels of KC and MCP-1 between treatment groups.

Natural killer (NK) cells are lymphocytes that do not require antigen-specificity like T cells to mount defenses against viruses and tumors[30]. After treatment with R-PDT or R-PDT + ∝PD-1, there was no change in the frequency of NK cells in the non-irradiated tumor (Figure 3, panel G). However, there was an increase in NK1.1+ cells in the spleen relative to PBS or ∝-PD-1 treated mice (Figure 3, panel H). The greater frequency of splenic NK cells after R-PDT or R-PDT + ∝PD-1, compared to PBS or ∝PD-1 treated mice suggests splenic NK cell proliferation and further re-affirms that R-PDT can induce a systemic innate immune response. Meanwhile, we did not observe any differences in NK cells in the non-irradiated tumor draining lymph nodes (Figure 3, panel I).

Repeated PDT alone and in combination with ∝PD-1 can systemically induce macrophage proliferation, and upregulate costimulatory molecules

Macrophages are leukocytes that phagocytose pathogens and have antigen-presentation functions to activate primed T cells[31]. In the non-irradiated tumor, there was a 1.7-fold and 1.8-fold increase in F4/80+CD11b+ macrophages after R-PDT + ∝PD-1, relative to PBS and R-PDT treated mice, respectively (Figure 4, panel A). No differences were observed in their expression of activation markers, such as MHC class II, CD80, or CD86 (Supplementary Figure 3, panels A, B, and C) between the treatment groups.

Meanwhile, in the spleen, we observed an increase in F4/80+CD11b+ splenic macrophages after treatment with R-PDT or R-PDT + ∝PD-1 compared to PBS or ∝PD-1 (Figure 4, panel B). Next, we investigated red pulp macrophages, a subset of which that are $CD11c_{int}$ can cross-prime conventional dendritic cells and present antigen to effector CD8+ T cells to mount an early antiviral response[32]. Quantification of this CD11b-F4/80+ $CD11c_{int}$ subset revealed no difference across treatment groups (Figure 4, panel C). Expression of MHC class II molecules was robust across treatment groups with expression on ~40% of CD11b-F4/80+ $CD11c_{int}$ cells (Figure 4, panel D). In addition, we observed greater expression of CD80 on CD11b-F4/80+ $CD11c_{int}$ cells after treatment with R-PDT + ∝PD-1 relative to PBS or ∝PD-1 treatment (Figure 4, panel E). Notably, expression of the co-stimulatory molecule CD86 was greater on CD11b-F4/80+ $CD11c_{int}$ cells after treatment with R-PDT relative to PBS or ∝PD-1 treatment, and for R-PDT + ∝PD-1 treated mice compared to PBS treated mice (Figure 4, panel F). With the presence of MHC class II molecules and upregulation of CD86 costimulatory molecules on these CD11b-F4/80+ $CD11c_{int}$ red pulp macrophages after R-PDT, these macrophages have the potential to cross-prime CD8+ T cells.

In the non-irradiated tumor draining lymph nodes, the percentage of F4/80-CD11b+ myeloid cells increased 1.7- and 1.8-fold after treatment with combination R-PDT + ∝PD-1 compared to PBS and ∝PD-1, respectively (Figure 4, panel G). In addition, this myeloid population had greater expression of MHC class II, after R-PDT or R-PDT + ∝PD-1 treatment, compared to PBS or ∝PD-1 (Figure 4, panel H). Neither expression of costimulatory CD80 nor CD86 differed between treatment groups (Supplementary Figure 3, panels D and E). Meanwhile, the percentage of F4/80+CD11b + macrophages also increased after R-PDT + ∝PD-1, relative to R-PDT and PBS (Supplementary Figure 3, panel F). MHC class II expression on medullary macrophages were similar across treatment groups (Supplementary Figure 3, panel G). CD80 expression was higher for R-PDT treated mice, compared to combination R-PDT + ∝PD-1 (Supplementary Figure 3, panel H). CD86 expression on F4/80+CD11b+ macrophages did not differ between treatment groups (Supplementary Figure 3, panel I). Given the increase in the frequency of myeloid cells after combination R-PDT + ∝PD-1, these subsets may contribute to antigen-presentation to T cells.

R-PDT and combination R-PDT + ∝PD-1 increased dendritic cell maturation

To bridge the innate and adaptive immune systems, activated dendritic cells process antigen for presentation to naïve T cells, resulting in the differentiation and proliferation of cognate T cells[33]. Upon activation, dendritic cells upregulate the antigen presentation marker, MHC class II, and costimulatory markers, CD80 and CD86.

In the non-irradiated tumor, there was an increase in the frequency of mature CD11c+ MHC class II+ dendritic cells in mice after combination R-PDT + ∝PD-1 treatment, relative to PBS (Figure 5, panel A). There were no changes in expression of CD80 or CD86 on CD11c+MHC class II+ dendritic cells between treatment groups (Figure 5, panels B and C). In the spleen, the frequencies of dendritic cells were similar across treatment groups (Figure 5, panel D). However, after R-PDT or combination R-PDT + ∝PD-1, there were 2.6- and 2.2-fold greater expression of the co-stimulatory marker, CD80, relative to PBS treated mice, respectively (Figure 5, panel E). CD86 was similarly upregulated on dendritic cells of mice treated with R-PDT or R-PDT + ∝PD-1, compared to PBS or ∝PD-1 (Figure 5, panel F). In the non-irradiated tumor draining-lymph nodes, we observed a 2.4- and 2.3-fold increase in mature CD11c+ MHC class II+ dendritic cells after R-PDT + ∝PD-1 treatment, relative to PBS or ∝PD-1 treatments (Figure 5, panel G). CD80+ and CD86+ expression on dendritic cells did not differ between treatment groups (Supplementary Figure 4, panels A and B). Across the non-irradiated tumor, spleen, and non-irradiated tumor draining lymph nodes, we observed the presence of dendritic cells that have antigen-presentation and costimulatory markers, which suggests their ability to prime CD4+ T cells.

R-PDT can alter CD3+ T cell populations systemically

CD3 is a pan-T cell marker and is found on CD4+ and CD8+ T cell subsets. CD4+ T cells play multi-faceted roles in anti-tumor immunity, including providing help to CD8+ T cells for cytolysis, help to B cells for antibody production, and secreting tumoricidal cytokines like IFN-γ[34]. Meanwhile, CD8+ T cells can directly eliminate tumor cells via binding of Fas receptors on tumor cells to activate death domains or by secreting cytotoxic molecules such as perforin and granzyme[35].

In the non-irradiated tumor, we observed a 2.4-fold increase in the percentage of CD3+ T cells after R-PDT + ∝PD-1 treatment relative to PBS (Figure 6, panels A and B), implying either greater proliferation of CD3+ T cells or migration from other organs. Delving into CD4+ and CD8+ T cell subsets, we did not note any differences between treatment groups (Figure 6, panels C and D). Further examination of the proportion of CD8+ naïve, central, and effector memory T cells subsets yielded no differences across treatment groups (Supplementary Figure 5, panels A, B, and C).

In the spleen, the proportion of CD3+ T cells declined 2.3-fold after R-PDT and R-PDT + ∝PD-1 treatment, compared to PBS treatment (Figure 6, panels E and F). This decline suggests that there is a migration of CD3+ T cells from the spleen after priming by dendritic cells and macrophages. Stratification of CD3+ T cells into CD4+ and CD8+ T cells revealed no differences between treatment groups (Figure 6, panels G and H). Stratification of CD8+ T cells by CD44 and CD62L into naïve and central memory T cells showed no difference across treatment groups (Supplementary Figure 5, panels D and E). Meanwhile, the frequency of CD8+CD44+CD62L- effector memory T cells was greater for combination R-PDT + ∝PD-1 treatment, relative to PBS treatment (Supplementary Figure 5, panel F).

Lastly, in the non-irradiated tumor draining lymph nodes, there were no differences in the proportions of CD3+ T cells across treatment groups (Figure 6, panels I and J). However, there

were shifts in the proportion of CD4+ and CD8+ T cells. There was a decline in the proportion of CD4+ T cells after R-PDT and R-PDT + ∝PD-1, compared to PBS or ∝PD-1 treatment (Figure 6, panel K). R-PDT resulted in a greater percentage of CD8+ T cells relative to PBS or ∝PD-1 treatment (Figure 6, panel L). Likewise, combination R-PDT + ∝PD-1 treatment yielded greater percentages of CD8+ T cells in the non-irradiated tumor draining lymph nodes, relative to ∝PD-1 treatment. The frequencies of CD8+ naïve, central memory, and effector memory subpopulations were similar across treatment groups (Supplementary Figure 5, panels G, H, I).

R-PDT, and R-PDT + ∝-PD-1 can shift CD4+ T cell subsets in the spleen and non-irradiated tumor draining lymph nodes

In the non-irradiated tumor, the proportions of naïve, central and effector memory CD4+ T cells, as well as CD4+ T_{regs}, were similar between treatment groups (Supplementary Figure 6). In the spleen, the proportions of naïve T cells did not differ between treatment groups (Figure 7, panels A and B). However, treatment with R-PDT resulted in a 1.4-fold reduction in the proportion of CD4+ central memory T cells compared to PBS (Figure 7, panel C). Similarly, combination R-PDT + ∝PD-1 induced a 1.6- and 1.4-fold reduction in the percentage of splenic CD4+ central memory T cells, relative to PBS and ∝PD-1, respectively. This reduction in the percentage of CD4+ central memory T cells was offset by a 2.0-fold increase in the proportion of CD4+ CD44+CD62L+ effector memory T cell after R-PDT, relative to PBS (Figure 7, panel D). Likewise, combination R-PDT + ∝PD-1 treatment also resulted in a 2.4-and 1.6-fold increase in CD4+ effector memory T cells, compared to PBS and ∝PD-1 treatment. After re-activation by antigen presenting cells, CD4+ central memory cells may differentiate and migrate to the non-irradiated tumor, accounting for the decline in the proportion of CD4+ central memory T cells after R-PDT and R-PDT + ∝PD-1 treatments. CD4+ T_{regs} are an immunosuppressive subset of T cells that maintain self-tolerance to prevent autoimmunity[36]. In the spleen, there was an increase in CD4+ T_{regs} after R-PDT or combination R-PDT + ∝PD-1 treatment compared to PBS or ∝PD-1 (Figure 7, panel E). This increase may arise as a counter-balance to splenic inflammation.

In the non-irradiated tumor-draining lymph node, the proportions of naïve and central memory CD4+ T cells were similar across treatment groups (Figure 7, panels F, G, and H). Delving into CD4+ T cell subsets, we observed that combination R-PDT + ∝PD-1 treatment resulted in a 1.7-fold higher proportion of CD44+CD62L+ effector memory T cells, compared to PBS treatment (Figure 7, panel I). Notably, there was a 1.4-fold decline in CD4+ T_{regs} in the non-irradiated tumor-draining lymph nodes after R-PDT compared to ∝PD-1 treatment, and 1.5-fold decrease for combination R-PDT + ∝PD-1 compared to both PBS or ∝PD-1 (Figure 7, panel J).

Despite systemic immune activation, CD4+ and CD8+ T cells do not infiltrate organs at higher rates after R-PDT compared to controls

Infiltration of CD4+ and CD8+ T cells into organs was investigated after mice were treated with PBS, ∝PD-1, R-PDT, or combination R-PDT + ∝PD-1. Immunohistology revealed no difference in CD4+ and CD8+ infiltration into the brain, colon, heart, kidney, liver, and lungs, between treatment groups (Figures 8 and 9). Accordingly, despite systemic immune activation, this lack of increase in CD4+ and CD8+ T-cell infiltration suggests a degree of safety and

reduced likelihood of immune related adverse events in major organs for R-PDT and combination R-PDT + ∝PD-1.

Liver and kidney function for mice treated with R-PDT + ∝PD-1

Liver and kidney function of mice were evaluated, from the serum obtained on Day 11. We did not observe any differences in total bilirubin or alanine aminotransferase between treatment groups (Figure 10, panels A and B). We noted a decline in alkaline phosphatase, after R-PDT relative to PBS or ∝PD-1 treated mice, and R-PDT + ∝PD-1 relative to PBS or ∝PD-1 treated mice (Figure 10, panel C). Alkaline phosphatase is an enzyme synthesized in the liver and bone, which removes phosphate groups in basic pH. Meanwhile, levels of blood urea nitrogen and creatinine were similar across treatment groups, suggesting normal kidney function (Figure 10, panels D and E).

Both serum potassium and phosphorus were higher for mice treated with combination R-PDT + ∝PD-1, relative to PBS (Figure 10, panels F and G). Lysis of tumor cells after combination R-PDT + ∝PD-1 with a subsequent release of intracellular potassium and phosphorus may account for the increases we observe[37,38]. Calcium and sodium were similar across treatment groups (Figure 10, panels H and I).

Next, we observed a 1.5- and 1.7-fold reduction in serum glucose for R-PDT and combination R-PDT + ∝PD-1, relative to PBS-treated mice (Figure 10, panel J). In parallel, we saw that treatment with R-PDT or combination R-PDT + ∝PD-1 reduced serum amylase in mice, compared to treatment with PBS (Figure 10, panel K). As serum amylase is an enzyme that hydrolyzes starch into glucose[39], a fall in serum amylase levels may reflect a reduction in the breakdown of starches into glucose.

Overall, R-PDT can induce alterations in liver enzymes, but combination R-PDT + ∝PD-1 may induce additional electrolyte alterations, including possible mild tumor cell lysis that result in spikes in electrolytes like phosphorus and potassium. However, body weight of mice across treatment groups did not differ, suggesting that these alterations may not have been clinically significant (Figure 10, panel L). Moreover, hematoxylin and eosin staining of organs including the brain, colon, heart, kidney, liver, and lungs, revealed no gross anatomical damage after R-PDT and combination R-PDT + ∝PD-1 relative to PBS-treated mice (Figure 111).

Discussion

Previously, we observed that R-PDT mediated by porphyrin lipoprotein (PLP) can induce the abscopal effect in a highly aggressive, dual subcutaneous AE17-OVA mesothelioma model in C57BL/6 mice[19]. Mice treated with R-PDT had a delay in non-irradiated tumor growth and improved survival, relative to controls. To understand why PLP mediated R-PDT alone can induce the abscopal effect, and how combination therapies strengthen the abscopal effect, we investigated the broader immune mechanisms facilitated by R-PDT and combination R-PDT + αPD-1 in dual AE17-OVA mesothelioma bearing mice. Then, we examined the safety profile of R-PDT and R-PDT + ∝PD-1.

Abscopal effect induced by R-PDT

The abscopal effect has been clinically observed in cancer patients treated with radiotherapy and its mechanisms there-in are better-characterized, relative to photodynamic therapy[40–43]. Mechanistically, the radiotherapy-induced abscopal effect involves immunogenic cell death upon irradiation of the primary tumor, recruitment of antigen-presenting cells to the irradiated tumor, T-cell priming by antigen presenting cells in the lymph nodes, and CD8+ T-cell mediated cytotoxicity against distant, non-treated tumor [44]. Similarly, in pre-clinical assessments of photodynamic therapy in combination with immune checkpoint blockade, the mechanisms of the abscopal effect also involve immunogenic cell death, CD8+ T-cell priming at the lymph nodes and migration of CD8+ T cells to distant, non-irradiated metastases or tumors [17,45]. In our work, we sought to more broadly evaluate the immune mechanisms underlying the immune response.

As previously described, treatment of primary AE17-OVA+ tumors with PLP-mediated PDT, resulted in a decrease in calreticulin expression in tumor tissue, suggestive of the release of this DAMP and the induction of immunogenic cell death[46]. In this work, we also report that after R-PDT relative to that of PBS-treated mice, we noted major differences systemically: 1) there was broad innate immune activation, and 2) there was likely antigen presentation by APCs in both the spleen and the non-irradiated tumor draining lymph node, which resulted in shifts in splenic CD4+ T cell populations, and an increase in nodal CD8+ T cells. A summary of the immune cross-talk is illustrated in Figure 12.

Many innate immune mechanisms appear to be activated by R-PDT. First, serum IL-6 was increased following R-PDT and combination R-PDT + ∝PD-1 (Figure 3, panel A). Others have reported increases in serum IL-6 following PDT. Gollnick et al. reported an increase in serum IL-6 and MIP-2 in EMT6 mammary tumor-bearing mice after a single round of HPPH-PDT[29]. Reginato et al. found an 18-fold increase in serum IL-6 in patients with esophageal squamous cell carcinomas after Photofrin-PDT for 7 days post PDT[47]. In addition, PDT using novel organic polymer nanoenzyme in B16F10 melanoma-bearing mice also resulted in 4.9-fold greater serum IL-6, relative to saline control at three days post-treatment[48]. Pro-inflammatory IL-6 triggers downstream effects which can include B cell activation and antibody production, which we likely observed in our study as an increase in serum globulins (Figure 3, panel C). Similarly, Preise et al. observed greater B cell infiltration in the tumor 24 hours after PDT with a Pd-bacteriochlorophyll derivatived photosensitizer in mice bearing CT26 colon carcinoma[49]. Accompanying this increase, they reported increased serum immunoglobulin titres one week post-PDT. The degree of importance to which B cell activation and globulin production is involved in the abscopal effect remains to be further investigated.

After R-PDT, we observed declines in serum levels of cytokines associated with neutrophil chemotaxis. IL-1∝, CXCL5, and MIP-2 were all reduced after R-PDT and combination R-PDT + ∝PD-1 treatments, relative to PBS treatment. Previously, de Vree et al[50], and Kousis et al.[51], have shown that after a single round of Photofrin-based and Photochlor-based PDT respectively, neutrophils were recruited to the tumor rapidly, where they regulate CD8+ T-cell proliferation in the tumor draining lymph nodes[51]. While neutrophils play an important role in the initiation of an anti-tumor response, with repeated rounds of PDT other immune cells may overtake the importance of neutrophils in sustaining long-term anti-tumor immune responses.

To bridge the innate and adaptive immune system, we hypothesize that R-PDT can induce antigen presentation in both the spleen and non-irradiated tumor draining lymph nodes. Destruction of the tumor by photodynamic therapy can induce release of DAMPs, heat shock proteins, and tumor antigens[8]. Previously, we showed that R-PDT altered levels of calreticulin at the irradiated tumor[19]. These DAMPs can attract leukocytes to the site of injury. Subsequently, antigen-presenting cells at the irradiated tumor may either migrate to the lymph nodes or spleen, or tumor antigens may enter the bloodstream and circulate to the spleen, where they are phagocytosed and processed by antigen presenting-cells. We found that dendritic cells in the spleen had upregulation of costimulatory molecules CD80 and CD86 after R-PDT, suggestive of CD4+ T cell mediated activation of antigen presenting cells via CD40-CD40L signalling (Figure 5, panels E and F). Meanwhile, splenic F4/80+CD11b+ myeloid cells were observed at a greater frequency after R-PDT or combination R-PDT + ∝PD-1, relative to ∝PD-1 or PBS treated mice (Figure 3, panel B). Moreover, red pulp macrophages with putative antigen presenting abilities had greater CD86 expression after R-PDT, relative to PBS-treated mice (Figure 3, panel F). Paralleling the increase in antigen presenting cells and their costimulatory marker expression, we noted a decrease in frequency of splenic CD3+ T cells, suggestive of their emigration (Figure 6, panels E and F). Within the CD4+ T-cell compartment, we observed a rise in the proportion of CD4+ effector memory T cells (Figure 7, panel D). Therefore, effector memory cells may be proliferating preferentially over central memory cells. The contribution of specific subsets of CD4+ T cells including T_{h1}, T_{h2}, and T_{h17} cells, remains to be elucidated.

Splenic DCs may also prime T_{regs}, as we observed a greater frequency of T_{regs} after treatment with R-PDT or combination R-PDT + ∝-PD-1, relative to PBS treated mice (Figure 7, panel E). Yamazaki et al. had previously reported that splenic dendritic cells can induce Foxp3+ T_{regs} in the presence of low amounts of OVA+ antigen and TGF-β[52,53]. Previously, in CT26 colorectal tumor-bearing mice, Reginato et al. observed an increase and peak in splenic T_{regs} four days after PDT, followed by a decline[54]. While the increase in percentage of splenic T_{regs} suggests that there could be an increase in the induction of tolerance to tumor antigens and subsequent attenuation of an anti-tumor response, the degree to which splenic T_{regs} retain their function is unknown. Reginato et al. reported that in squamous cell carcinoma patients, PDT reduced the suppressive capacity of peripheral T_{regs} without affecting the frequency of T_{regs} and suggested that the attenuation in T_{reg} function could be mediated by an increase in serum IL-6[47]. In our work, we observed an increase in serum IL-6, which may also have downstream effects that downregulate splenic T_{reg} function (Figure 3, panel A). T_{regs} can secrete inhibitory cytokines including IL-10, but we did not observe any accompanying increases in serum IL-10 after R-PDT or combination R-PDT + ∝PD-1 treatment, compared to PBS (Supplementary Figure 1, panel H). The functionality of splenic T_{regs} after PDT, and their role in anti-tumor immunity can be further investigated.

In the non-irradiated tumor draining lymph nodes, we found an increase in the frequency of CD8+ T cells, whereas CD4+ T cell frequency was reduced after R-PDT compared to PBS treated mice (Figure 6, panels K and L). This suggests the proliferation of CD8+ T cells, possibly arising from a combination of dendritic cell cross-presentation or CD4+ T cell help[34].

Abscopal effect induced by combination R-PDT + ∝PD-1

Combination R-PDT + ∝PD-1 induced similar immune responses as R-PDT, namely: 1) broad innate immune activation with higher serum IL-6 and globulins (Figure 3), 2) greater antigen presentation in the spleen, with dendritic cells upregulating CD80 and CD86 (Figure 5, panels E and F) and red pulp macrophages with increased CD86 expression (Figure 3, panel E), 3) decline in the percentage of splenic CD3+ T cells, implying T cell emigration away from the spleen (Figure 6, panels E and F), 4) alterations to CD4+ T cell subsets, with a decline in central memory T cells, and a rise in effector memory plus T_{regs} in the spleen (Figure 7, panels A to E), and 5) reduction in CD4+ T cells in the non-irradiated tumor draining lymph nodes (Figure 6, panels I and K) with a reduced proportion of T_{regs} (Figure 7, panel J).

In addition, combination R-PDT + ∝PD-1 induced other responses relative to PBS or ∝PD-1 treated mice, including: 1) increase in natural killer cells in the spleen (Figure 3, panel H), 2) an increase in F4/80-CD11b+ myeloid cells in the non-irradiated tumor draining lymph nodes and accompanying greater expression of MHC class II (Figure 4, panels G and H), 3) in the non-irradiated tumor draining lymph nodes, there were greater percentages of dendritic cells suggestive of priming of naïve T cells (Figure 5, panel G), 4) at the distal, non-irradiated tumor, there was an increase in the percentage of dendritic cells (Figure 5, panel A) and macrophages (Figure 4, panel A), which can prime effector T cells, and 5) at the distal tumor, there was an increase in CD3+ T cells (Figure 6, panels A and B), which may arise from the proliferation of primed effector T cells.

We found that the frequency of splenic natural killer cells increased after combination R-PDT + ∝PD-1 relative to PBS treated mice (Figure 3, panel H). Previously, Kabingu et al. reported that in mice bearing subcutaneous EMT6 and EMT6 lung tumours treated with Photofrin-PDT, depletion of NK cells resulted in the inability of PDT to reduce non-irradiated lung tumors[55]. They postulated that NK cells provide help to CD8+ T cells, to help modulate distal tumor growth. Given the crosstalk between natural killer cells and macrophages and dendritic cells, an increase in the frequency of NK cells may further promote cross-talk, with downstream macrophage and dendritic cell activation.

In the tumor draining lymph nodes of the non-irradiated, distal tumor, there was an increase in the proportion of F4/80-CD11b+ myeloid cells after combination R-PDT + ∝PD-1 and an upregulation of MHC class II expression (Figure 4, panels G and H), suggestive of their activation. This population includes subcapsular macrophages, which are the first immune cells to encounter and sample antigens in lymph from incoming afferent vessels[56]. Activated subcapsular macrophages have been shown to provide antigen directly to follicular B cells and promote antibody affinity maturation[57–59]. As such, subcapsular macrophage crosstalk with B cells may also contribute to our observation of increased serum globulins after combination R-PDT + ∝PD-1 relative to PBS-treated mice.

At the distal, non-irradiated tumor, treatment of mice with combination R-PDT + ∝PD-1, resulted in an increase in both dendritic cells (Figure 5, panel A) and macrophages (Figure 4 panel A), compared to PBS-treated mice. In parallel, there was an increase in CD3+ T cells (Figure 6, panels A and B) suggestive of T cell proliferation after priming by antigen presenting cells.

Safety profiles of R-DPT and combination R-PDT + ∝PD-1

Given the systemic immune activation induced by R-PDT and potential for immune-related adverse events with the addition of ∝PD-1 to R-PDT, we investigated the safety of R-PDT and combination R-PDT + ∝PD-1 relative to monotherapy ∝PD-1 and PBS treatment. Relative to ∝PD-1 and PBS-treated mice, treatment with R-PDT resulted in a similar infiltration of CD4+ and CD8+ T cells in into critical organs, such as the brain, colon, heart, kidney, liver, and lungs (Figures 8 and 9). Likewise, combination R-PDT + ∝PD-1 had no difference in CD4+ and CD8+ T cell infiltration in the brain, colon, heart, kidney, liver, and lungs, compared to ∝PD-1 and PBS. Moreover, no differences in CD4+ and CD8+ T cell infiltration were detected between R-PDT and combination R-PDT + ∝PD-1 in the aforementioned organs. Therefore, the addition of ∝PD-1 may not induce additional cytotoxicities over R-PDT, and the likelihood of immune-related adverse events in these major organs after R-PDT and combination R-PDT+ ∝PD-1 may be low.

Relative to mice treated with PBS, there was reduced serum glucose after R-PDT and combination R-PDT+ ∝PD-1, which was accompanied by a reduction in serum amylase that breaks down starches to glucose (Figure 10, panels J and K). After R-PDT and combination R-PDT+ ∝PD-1, we observed that liver function may be altered, as there was a decline in serum alkaline phosphatase relative to PBS-treated mice (Figure 10, panel C), while total bilirubin and alanine aminotransferase levels were similar across treatment groups (Figure 10, panel A and B). After R-PDT, kidney function appeared normal, as blood urea nitrogen and creatinine, serum phosphorus and potassium were also similar across groups (Figure 10, panel D and E). However, for combination R-PDT+ ∝PD-1 treated mice, there were increases in serum phosphorus and potassium (Figure 10, panels F and G). Taken together with the non-different calcium and creatinine levels, this rise in phosphorus and potassium is consistent with mild laboratory tumor cell lysis syndrome[37]. Accordingly, R-PDT appears to be well-tolerated and may have fewer side effects compared to combination R-PDT+ ∝PD-1.

Here, we aimed to provide a broader framework to show the crosstalk between various immune cells after R-PDT and combination R-PDT+ ∝PD-1 across the spleen, non-irradiated tumor-draining lymph node, and distal non-irradiated tumor, and blood. Moreover, we showed a promising safety profile for R-PDT. However, the following limitations are noted: first, we examined one timepoint after R-PDT; additional, longitudinal assessments may reveal other differences between treatment groups. Second, there are likely to be differences in in vivo immune responses, depending on the photosensitizer type, dosage, and fluence[2,60–62], as differences amongst these parameters can affect the degree by which immunogenic cell death and subsequent immune activation is initiated. Third, there may be differences in immune crosstalk that underlie the abscopal effect in different tumor models. Tumors have been classified as immunologically “cold” or “hot” based on their degree of CD3+ and CD8+ T cell infiltration[63]. In hot tumors, we anticipate that the systemic antigen presentation induced by R-PDT could potentiate and increase the magnitude of T cell cytotoxicity against non-irradiated tumors, boosting the abscopal effect.

While monotherapy photodynamic therapy and monotherapy immune checkpoint blockade are approved to treat various tumors, there is presently a dearth of clinical trials that evaluate the safety and efficacy of combination photodynamic therapy and ∝PD-1. From a search on

clinicaltrials.gov, there is currently one such clinical trial, which evaluates toxicities after a single round of 5-aminolevulinic acid (5-ALA) mediated intrapleural photodynamic therapy in combination with nivolumab for individuals with mesothelioma. If R-PDT alone, or in combination with immune checkpoint blockade is effective in generating an abscopal effect, both could be a great option for patients ineligible for surgery. Compared to standard therapies such as chemotherapy and radiotherapy, R-PDT alone or combination PDT with immune checkpoint blockade is advantageous in that both treatments are minimally invasive, and can help control distant tumors, while potentially generating immune memory and preventing recurrences. Understanding the mechanisms by which the abscopal effect can occur and the safety of combination therapy can facilitate the clinical translation of combination PDT with immune checkpoint blockade. Our findings suggest that the abscopal effect involves: 1) the release of calreticulin, a DAMP, from the irradiated tumor[19], 2) activation of innate immune system such as IL-6 which triggers downstream immunity, 3) antigen-presentation at the spleen by red pulp macrophages and dendritic cells to CD4+ T cells, which subsequently emigrate, and antigen presentation at the lymph nodes by dendritic cells to CD8+ T cells. Promisingly, after R-PDT and combination R-PDT + ∝-PDT, we did not observe major toxicities of concern.

However, further investigations into different photosensitizer types, treatment schedules, and tumor models are warranted, to determine how these factors affect the immune response underlying the abscopal effect and corresponding safety profile. As our understanding of how PDT systemically induces the abscopal effect improves, we will advance the utility of PDT as a treatment for advanced, disseminated tumors.

Acknowledgements
The authors thank Deborah Scollard, Teesha Komal, and Azza Al Mahrouki for their assistance. The authors also acknowledge the Centre for Pharmaceutical Oncology and STTARR Innovation Centre for use of facilities and STTARR Pathology Core for their services.

Declaration of competing interest
The authors declare no competing interests.

Credit Author Statement
JL - conceptualization, formal analysis, investigation, methodology, writing - original draft, review, editing; **MA** - conceptualization, investigation, methodology, writing - review and editing; **NB** - conceptualization, investigation, writing - review and editing; **TC** - investigation, writing- review and editing; **AG** - investigation, writing - review and editing; **YH** - investigation, writing- review and editing; **TI** - investigation, writing- review and editing; **CL** - investigation, writing – review and editing; **LD** - investigation, writing – reviewing and editing; **SK** - writing- review and editing; **TK**- writing- review and editing; **YS** - writing- review and editing; **HO** - writing- review and editing; **JC** - resources, investigation, writing - review & editing; **TK** - writing- review and editing; **KY** - resources, writing -review & editing, supervision, funding acquisition; **GZ** - resources, writing - review & editing, supervision, funding acquisition.

Funding
This study was funded by the Terry Fox Research Institute (Grant No. PPG-1075), William Coco Chair in Surgical Innovation for Lung Cancer, the Surgical Innovation for Lung Cancer Fund for

Excellence, JSPS KAKENHI (Grant Number JP18KK0457), the Canadian Institute of Health Research (Foundation Grant #154326), the Natural Sciences and Engineering Research Council of Canada (no. 386613), the Canada Research Chair Programs, and the Princess Margaret Cancer Foundation.

References

1. Kessel D, Oleinick NL. Cell Death Pathways Associated with Photodynamic Therapy: An Update. *Photochem Photobiol*. 2018;94(2):213-218. doi:10.1111/PHP.12857
2. Garg AD, Agostinis P. ER stress, autophagy and immunogenic cell death in photodynamic therapy-induced anti-cancer immune responses. *Photochem Photobiol Sci 2014 133*. 2014;13(3):474-487. doi:10.1039/C3PP50333J
3. Nath S, Obaid G, Hasan T. The Course of Immune Stimulation by Photodynamic Therapy: Bridging Fundamentals of Photochemically Induced Immunogenic Cell Death to the Enrichment of T-Cell Repertoire. *Photochem Photobiol*. 2019;95(6):1288-1305. doi:10.1111/PHP.13173
4. Gunaydin G, Gedik ME, Ayan S. Photodynamic Therapy for the Treatment and Diagnosis of Cancer–A Review of the Current Clinical Status. *Front Chem*. 2021;9:608. doi:10.3389/FCHEM.2021.686303/BIBTEX
5. Ghosh P, Hanada Y, Linn B, Mangels-Dick T, Roy B, Wang K. S1479 Abscopal Effect of Intratumoral Photodynamic Therapy Is Associated with Increased Tumor Directed T Cells. *Am J Gastroenterol*. 2021;116(1):S676-S677. doi:10.14309/01.AJG.0000779448.16118.B1
6. Maeding N, Verwanger T, Krammer B. Boosting Tumor-Specific Immunity Using PDT. *Cancers (Basel)*. 2016;8(10). doi:10.3390/CANCERS8100091
7. Garg AD, Krysko D V., Vandenabeele P, Agostinis P. DAMPs and PDT-mediated photo-oxidative stress: exploring the unknown. *Photochem Photobiol Sci*. 2011;10(5):670-680. doi:10.1039/C0PP00294A
8. Hwang HS, Shin H, Han J, Na K. Combination of photodynamic therapy (PDT) and anti-tumor immunity in cancer therapy. *J Pharm Investig*. 2018;48(2):143. doi:10.1007/S40005-017-0377-X
9. Li X, Lovell JF, Yoon J, Chen X. Clinical development and potential of photothermal and photodynamic therapies for cancer. *Nat Rev Clin Oncol*. 2020;17(11):657-674. doi:10.1038/s41571-020-0410-2
10. Kwon N, Kim H, Li X, Yoon J. Supramolecular agents for combination of photodynamic therapy and other treatments. *Chem Sci*. 2021;12(21):7248-7268. doi:10.1039/d1sc01125a
11. Xu J, Xu L, Wang C, et al. Near-Infrared-Triggered Photodynamic Therapy with Multitasking Upconversion Nanoparticles in Combination with Checkpoint Blockade for Immunotherapy of Colorectal Cancer. *ACS Nano*. 2017;11(5):4463-4474. doi:10.1021/acsnano.7b00715
12. Wang Z, Zhang F, Shao D, et al. Janus Nanobullets Combine Photodynamic Therapy and Magnetic Hyperthermia to Potentiate Synergetic Anti-Metastatic Immunotherapy. *Adv Sci*. 2019;6(22):1901690. doi:10.1002/ADVS.201901690
13. Li X, Jeon YH, Kwon N, et al. In Vivo-assembled phthalocyanine/albumin supramolecular complexes combined with a hypoxia-activated prodrug for enhanced photodynamic immunotherapy of cancer. *Biomaterials*. 2021;266(May 2020):120430. doi:10.1016/j.biomaterials.2020.120430

14. Wang R, Kim KH, Yoo J, et al. A Nanostructured Phthalocyanine/Albumin Supramolecular Assembly for Fluorescence Turn-On Imaging and Photodynamic Immunotherapy. *ACS Nano*. 2022;16(2):3045-3058. doi:10.1021/acsnano.1c10565
15. Duan X, Chan C, Guo N, Han W, Weichselbaum RR, Lin W. Photodynamic Therapy Mediated by Nontoxic Core-Shell Nanoparticles Synergizes with Immune Checkpoint Blockade To Elicit Antitumor Immunity and Antimetastatic Effect on Breast Cancer. *J Am Chem Soc*. 2016;138(51):16686-16695. doi:10.1021/JACS.6B09538/SUPPL_FILE/JA6B09538_SI_001.PDF
16. Wang D, Wang T, Liu J, et al. Acid-Activatable Versatile Micelleplexes for PD-L1 Blockade-Enhanced Cancer Photodynamic Immunotherapy. *Nano Lett*. 2016;16(9):5503-5513. doi:10.1021/ACS.NANOLETT.6B01994/ASSET/IMAGES/LARGE/NL-2016-01994D_0004.JPEG
17. He C, Duan X, Guo N, et al. Core-shell nanoscale coordination polymers combine chemotherapy and photodynamic therapy to potentiate checkpoint blockade cancer immunotherapy. *Nat Commun 2016 71*. 2016;7(1):1-12. doi:10.1038/ncomms12499
18. Cui L, Lin Q, Jin CS, et al. A PEGylation-Free biomimetic porphyrin banoplatform for personalized cancer theranostics. *ACS Nano*. 2015;9(4):4484-4495. doi:10.1021/ACSNANO.5B01077/SUPPL_FILE/NN5B01077_SI_001.PDF
19. Lou J, Aragaki M, Bernards N, et al. Repeated porphyrin lipoprotein-based photodynamic therapy controls distant disease in mouse mesothelioma via the abscopal effect. *Nanophotonics*. 2021;10(12):3279-3294. doi:10.1515/NANOPH-2021-0241/DOWNLOADASSET/SUPPL/J_NANOPH-2021-0241_SUPPL.DOCX
20. Seidel JA, Otsuka A, Kabashima K. Anti-PD-1 and anti-CTLA-4 therapies in cancer: Mechanisms of action, efficacy, and limitations. *Front Oncol*. 2018;8(MAR):86. doi:10.3389/FONC.2018.00086/BIBTEX
21. Twomey JD, Zhang B. Cancer Immunotherapy Update: FDA-Approved Checkpoint Inhibitors and Companion Diagnostics. *AAPS J*. 2021;23(2). doi:10.1208/S12248-021-00574-0
22. Abdul Rahim SN, Ho GY, Coward JIG. The role of interleukin-6 in malignant mesothelioma. *Transl Lung Cancer Res*. 2015;4(1):55. doi:10.3978/J.ISSN.2218-6751.2014.07.01
23. Tanaka T, Narazaki M, Kishimoto T. IL-6 in Inflammation, Immunity, and Disease. *Cold Spring Harb Perspect Biol*. 2014;6(10):a016295. doi:10.1101/CSHPERSPECT.A016295
24. Capucetti A, Albano F, Bonecchi R. Multiple Roles for Chemokines in Neutrophil Biology. *Front Immunol*. 2020;11:1259. doi:10.3389/FIMMU.2020.01259/BIBTEX
25. Di Paolo NC, Shayakhmetov DM. Interleukin 1α and the inflammatory process. *Nat Immunol 2016 178*. 2016;17(8):906-913. doi:10.1038/ni.3503
26. Rider P, Carmi Y, Guttman O, et al. IL-1α and IL-1β Recruit Different Myeloid Cells and Promote Different Stages of Sterile Inflammation. *J Immunol*. 2011;187(9):4835-4843. doi:10.4049/JIMMUNOL.1102048
27. Hu B, Fan H, Lv X, Chen S, Shao Z. Prognostic significance of CXCL5 expression in cancer patients: A meta-analysis. *Cancer Cell Int*. 2018;18(1):1-12. doi:10.1186/S12935-018-0562-7/FIGURES/6
28. Masucci MT, Minopoli M, Carriero MV. Tumor Associated Neutrophils. Their Role in Tumorigenesis, Metastasis, Prognosis and Therapy. *Front Oncol*. 2019;9:1146. doi:10.3389/FONC.2019.01146

29. Gollnick SO, Evans SS, Baumann H, et al. Role of cytokines in photodynamic therapy-induced local and systemic inflammation. *Br J Cancer*. 2003;88(11):1772. doi:10.1038/SJ.BJC.6600864
30. Abel AM, Yang C, Thakar MS, Malarkannan S. Natural killer cells: Development, maturation, and clinical utilization. *Front Immunol*. 2018;9(AUG):1869. doi:10.3389/FIMMU.2018.01869/BIBTEX
31. Jackaman C, Yeoh TL, Acuil ML, Gardner JK, Nelson DJ. Murine mesothelioma induces locally-proliferating IL-10+TNF-α+CD206−CX3CR1+ M3 macrophages that can be selectively depleted by chemotherapy or immunotherapy. *Oncoimmunology*. 2016;5(6). doi:10.1080/2162402X.2016.1173299/SUPPL_FILE/KONI_A_1173299_SM2837.PDF
32. Enders M, Franken L, Philipp M-S, et al. Splenic Red Pulp Macrophages Cross-Prime Early Effector CTL That Provide Rapid Defense against Viral Infections. *J Immunol*. 2020;204(1):87-100. doi:10.4049/JIMMUNOL.1900021/-/DCSUPPLEMENTAL
33. Gardner A, de Mingo Pulido Á, Ruffell B. Dendritic Cells and Their Role in Immunotherapy. *Front Immunol*. 2020;11:924. doi:10.3389/FIMMU.2020.00924/BIBTEX
34. Tay RE, Richardson EK, Toh HC. Revisiting the role of CD4+ T cells in cancer immunotherapy—new insights into old paradigms. *Cancer Gene Ther 2020 281*. 2020;28(1):5-17. doi:10.1038/s41417-020-0183-x
35. Raskov H, Orhan A, Christensen JP, Gögenur I. Cytotoxic CD8+ T cells in cancer and cancer immunotherapy. *Br J Cancer 2020 1242*. 2020;124(2):359-367. doi:10.1038/s41416-020-01048-4
36. Kumar P, Bhattacharya P, Prabhakar BS. A comprehensive review on the role of co-signaling receptors and Treg homeostasis in autoimmunity and tumor immunity. *J Autoimmun*. 2018;95:77-99. doi:10.1016/J.JAUT.2018.08.007
37. Howard SC, Jones DP, Pui C-H. The Tumor Lysis Syndrome. *N Engl J Med*. 2011;364(19):1844. doi:10.1056/NEJMRA0904569
38. Cairo MS, Bishop M. Tumour lysis syndrome: new therapeutic strategies and classification. *Br J Haematol*. 2004;127(1):3-11. doi:10.1111/J.1365-2141.2004.05094.X
39. Akinfemiwa O, Muniraj T. Amylase. *StatPearls*. July 2021. https://www.ncbi.nlm.nih.gov/books/NBK557738/. Accessed August 10, 2022.
40. Kingsley DPE. An interesting case of possible abscopal effect in malignant melanoma. *Br J Radiol*. 1975;48(574):863-866. doi:10.1259/0007-1285-48-574-863
41. Ehlers G, Fridman M. Abscopal effect of radiation in papillary adenocarcinoma. *Br J Radiol*. 1973;46(543):220-222. doi:10.1259/0007-1285-46-543-220
42. MacManus MP, Harte RJ, Stranex S. Spontaneous regression of metastatic renal cell carcinoma following palliative irradiation of the primary tumour. *Ir J Med Sci*. 1994;163(10):461-463. doi:10.1007/BF02940567
43. Ohba K, Omagari K, Nakamura T, et al. Abscopal regression of hepatocellular carcinoma after radiotherapy for bone metastasis. *Gut*. 1998;43(4):575-577. doi:10.1136/GUT.43.4.575
44. Ngwa W, Irabor OC, Schoenfeld JD, Hesser J, Demaria S, Formenti SC. Using immunotherapy to boost the abscopal effect. *Nat Rev Cancer 2018 185*. 2018;18(5):313-322. doi:10.1038/nrc.2018.6
45. Duan X, Chan C, Guo N, Han W, Weichselbaum RR, Lin W. Photodynamic Therapy Mediated by Nontoxic Core-Shell Nanoparticles Synergizes with Immune Checkpoint

Blockade To Elicit Antitumor Immunity and Antimetastatic Effect on Breast Cancer. *J Am Chem Soc*. 2016;138(51):16686-16695. doi:10.1021/JACS.6B09538
46. Lou J, Aragaki M, Bernards N, et al. Repeated porphyrin lipoprotein-based photodynamic therapy controls distant disease in mouse mesothelioma via the abscopal effect. *Nanophotonics*. 2021;10(12):3279-3294. doi:10.1515/NANOPH-2021-0241/PDF
47. Reginato E, Lindenmann J, Langner C, et al. Photodynamic therapy downregulates the function of regulatory T cells in patients with esophageal squamous cell carcinoma. *Photochem Photobiol Sci 2014 139*. 2014;13(9):1281-1289. doi:10.1039/C4PP00186A
48. Zeng Z, Zhang C, Li J, et al. Activatable Polymer Nanoenzymes for Photodynamic Immunometabolic Cancer Therapy. *Adv Mater*. 2021;33(4):2007247. doi:10.1002/ADMA.202007247
49. Preise D, Oren R, Glinert I, et al. Systemic antitumor protection by vascular-targeted photodynamic therapy involves cellular and humoral immunity. *Cancer Immunol Immunother*. 2009;58(1):71-84. doi:10.1007/S00262-008-0527-0
50. De Vree WJA, Essers MC, De Bruijn HS, Star WM, Koster JF, Sluiter2 W. Evidence for an Important Role of Neutrophils in the Efficacy of Photodynamic Therapy in Vivo1. *CANCER Res*. 1996;56:2908-2911. http://aacrjournals.org/cancerres/article-pdf/56/13/2908/2460794/cr0560132908.pdf. Accessed May 12, 2022.
51. Kousis PC, Henderson BW, Maier PG, Gollnick SO. Photodynamic Therapy Enhancement of Antitumor Immunity Is Regulated by Neutrophils. *Cancer Res*. 2007;67(21):10501-10511. doi:10.1158/0008-5472.CAN-07-1778
52. Yamazaki S, Bonito AJ, Spisek R, Dhodapkar M, Inaba K, Steinman RM. Dendritic cells are specialized accessory cells along with TGF-β for the differentiation of Foxp3+ CD4+ regulatory T cells from peripheral Foxp3− precursors. *Blood*. 2007;110(13):4293-4302. doi:10.1182/BLOOD-2007-05-088831
53. Yamazaki S, Dudziak D, Heidkamp GF, et al. CD8+CD205+ Splenic Dendritic Cells Are Specialized to Induce Foxp3+ Regulatory T Cells. *J Immunol*. 2008;181(10):6923-6933. doi:10.4049/JIMMUNOL.181.10.6923
54. Reginato E, Mroz P, Chung H, Kawakubo M, Wolf P, Hamblin MR. Photodynamic therapy plus regulatory T-cell depletion produces immunity against a mouse tumour that expresses a self-antigen. *Br J Cancer 2013 1098*. 2013;109(8):2167-2174. doi:10.1038/bjc.2013.580
55. Kabingu E, Vaughan L, Owczarczak B, Ramsey KD, Gollnick SO. CD8+ T cell-mediated control of distant tumours following local photodynamic therapy is independent of CD4+ T cells and dependent on natural killer cells. *Br J Cancer*. 2007;96(12):1839. doi:10.1038/SJ.BJC.6603792
56. Louie DAP, Liao S. Lymp node subcapsular sinus macrophages as the frontline of lymphatic immune defense. *Front Immunol*. 2019;10(FEB):347. doi:10.3389/FIMMU.2019.00347/BIBTEX
57. Carrasco YR, Batista FD. B cells acquire particulate antigen in a macrophage-rich area at the boundary between the follicle and the subcapsular sinus of the lymph node. *Immunity*. 2007;27(1):160-171. doi:10.1016/J.IMMUNI.2007.06.007
58. Gaya M, Castello A, Montaner B, et al. Inflammation-induced disruption of SCS macrophages impairs B cell responses to secondary infection. *Science (80-)*. 2015;347(6222):667-672. doi:10.1126/SCIENCE.AAA1300/SUPPL_FILE/GAYA.SM.PDF

59. Phan TG, Green JA, Xu Y, Cyster JG. Immune complex relay by subcapsular sinus macrophages and noncognate B cells drives antibody affinity maturation. *Nat Immunol*. 2009;10(7):786-796. doi:10.1038/NI.1745
60. Henderson BW, Gollnick SO, Snyder JW, et al. Choice of oxygen-conserving treatment regimen determines the inflammatory response and outcome of photodynamic therapy of tumors. *Cancer Res*. 2004;64(6):2120-2126. doi:10.1158/0008-5472.CAN-03-3513
61. Shams M, Owczarczak B, Manderscheid-Kern P, Bellnier DA, Gollnick SO. Development of photodynamic therapy regimens that control primary tumor growth and inhibit secondary disease. *Cancer Immunol Immunother*. 2015;64(3):287-297. doi:10.1007/S00262-014-1633-9
62. Falk-Mahapatra R, Gollnick SO. Photodynamic Therapy and Immunity: An Update. *Photochem Photobiol*. 2020;96(3):550-559. doi:10.1111/PHP.13253
63. Galon J, Bruni D. Approaches to treat immune hot, altered and cold tumours with combination immunotherapies. *Nat Rev Drug Discov 2018 183*. 2019;18(3):197-218. doi:10.1038/S41573-018-0007-Y

Figures

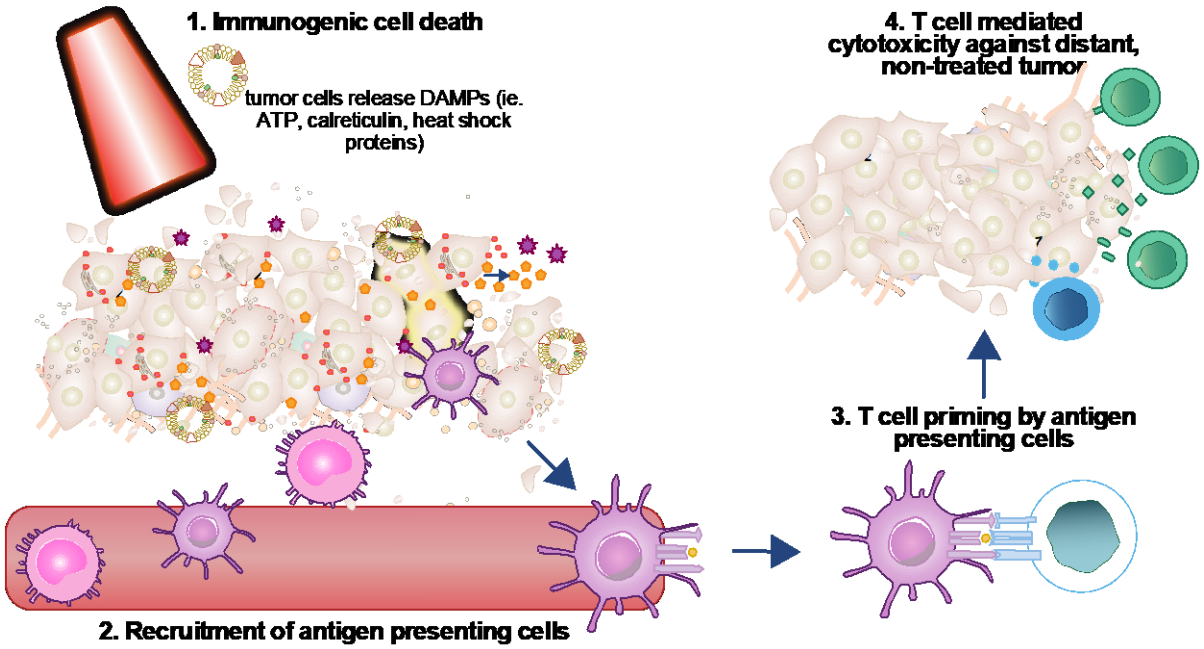

Figure 1. Overview of the mechanisms of the abscopal effect.

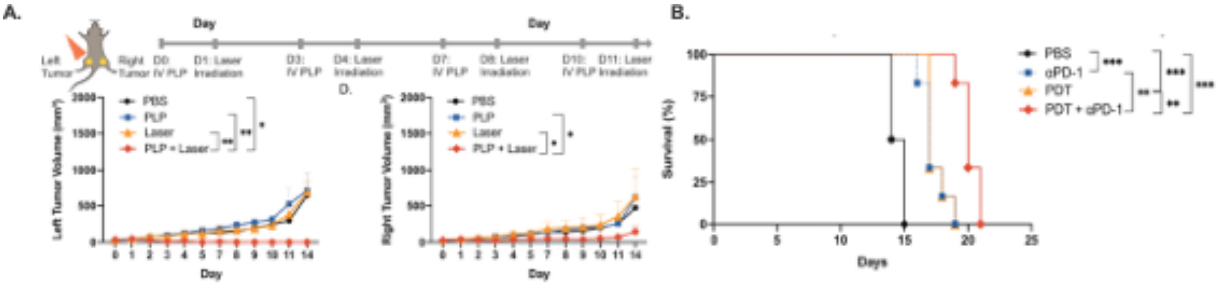

C.

Treatment Groups:

a) PBS
b) αPD-1 (12 mg/kg)
c) R-PDT (PLP at 4 mg/kg)
d) Combination αPD-1 (12 mg/kg) + R-PDT (PLP at 4 mg/kg)

Treatment Schedule

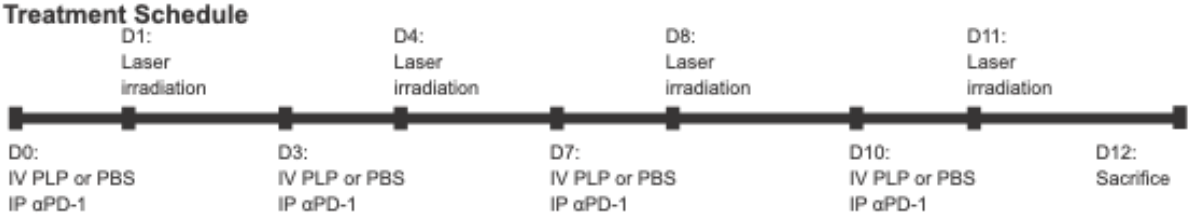

Assessments:

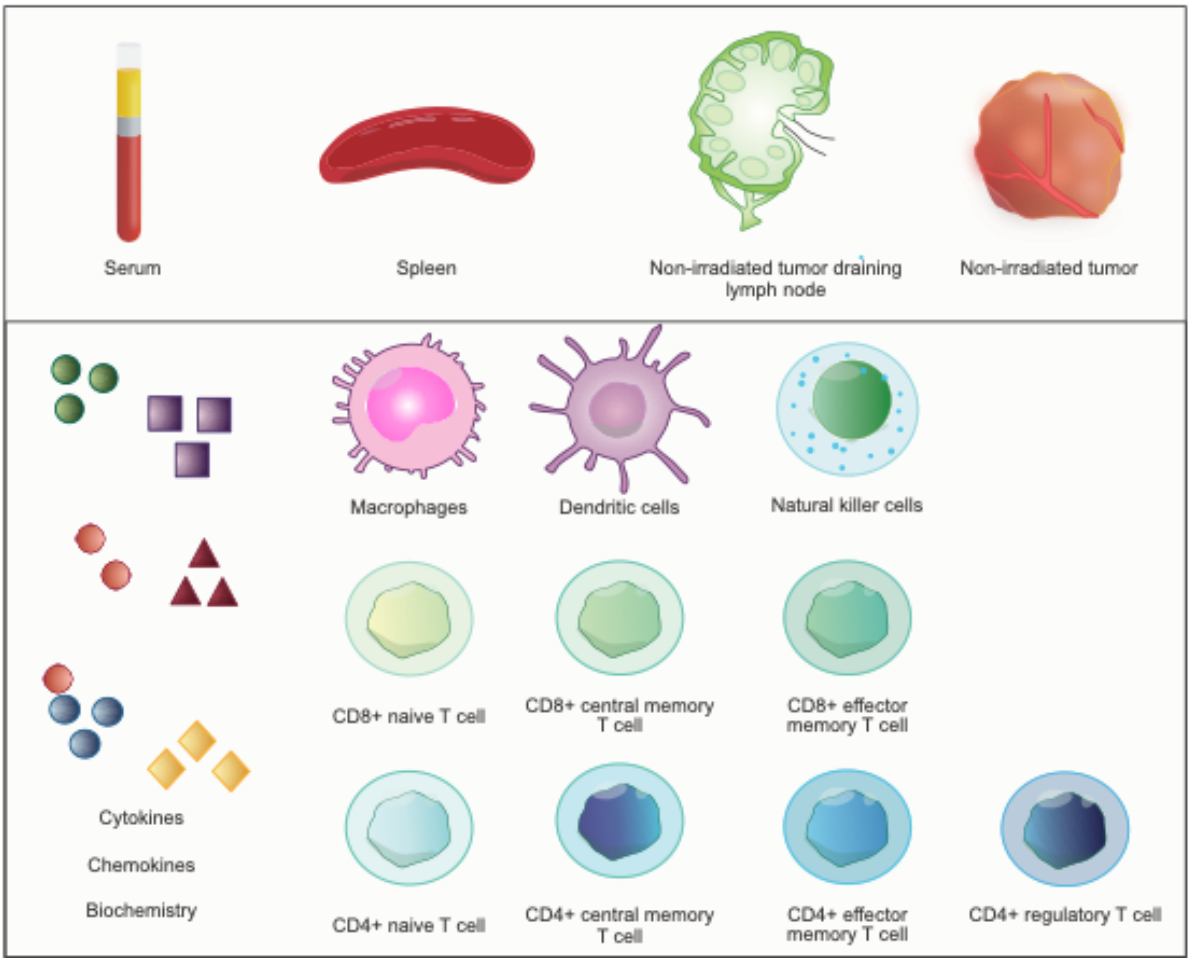

Figure 2. Overview of study. Our previously published work showed that porphyrin lipoprotein (PLP) mediated PDT can induce the abscopal effect, when performed four times. Dual subcutaneous AE17-OVA+ tumor bearing mice were treated with four cycles of PBS, PLP (4 mg/kg), laser irradiation at 50 J/cm^2, or PDT (PLP + laser). In (A), tumor volumes for irradiated, left tumors and non-irradiated right tumors are shown on the left and right, respectively. In (B), the survival of mice that were treated with four cycles of PBS, αPD-1 antibody (12 mg/kg), PDT (PLP at 4 mg/kg), or combination αPD-1 antibody (12 mg/kg) and PDT (PLP at 4 mg/kg) are shown. Data are mean ± standard deviation. Statistical significance of the survival of mice was determined using a one-way ANOVA, followed by a post hoc Tukey test ($n = 5$, $^{**}p < 0.01$, $^{***}p < 0.001$). Reproduced with permission from Lou et al. Nanophotonics 2021. The present study to evaluate the immune mechanisms underlying the abscopal effect with and without immune checkpoint inhibitor is outlined in (C). Dual subcutaneous AE17-OVA mesothelioma tumor bearing female mice received one of four treatments: phosphate buffered saline (PBS), anti-PD-1 monoclonal antibody (∝PD-1), repeated photodynamic therapy (R-PDT), or combination R-PDT + ∝PD-1, as per the illustrated treatment schedule. On Day 11, mice were sacrificed and the right, non-irradiated tumor, spleen, and non-irradiated tumor draining lymph nodes were dissected for analysis of several immune cell populations. Serum was obtained to evaluate cytokines, chemokines, as well as liver and kidney enzymes and electrolytes.

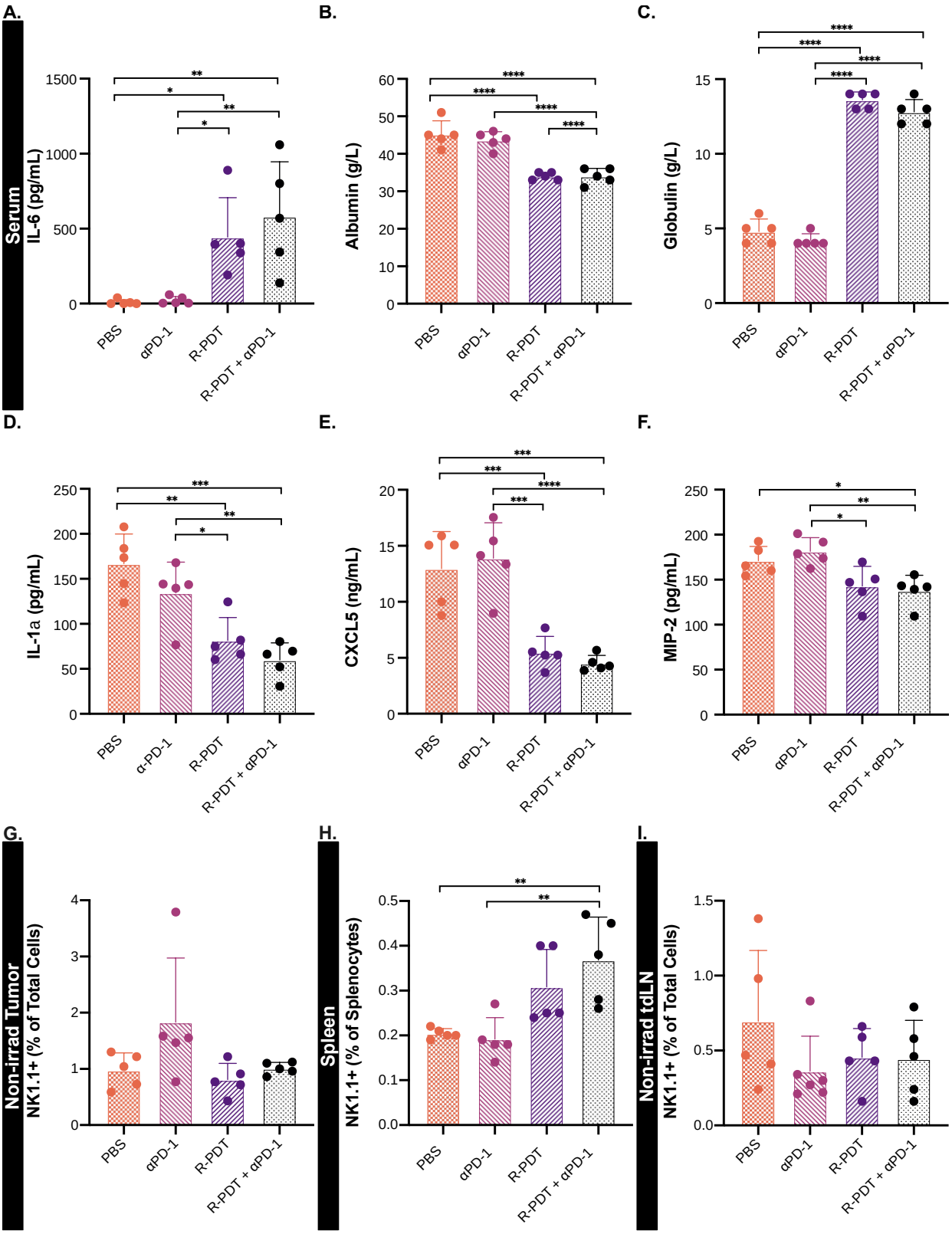

Figure 3. Activation of the innate immune system after repeated photodynamic therapy (R-PDT) and combination R-PDT + anti-PD-1 monoclonal antibody (∝PD-1). Serum was obtained from

mice after treatment with either phosphate buffered saline (PBS), ∝PD-1, R-PDT, or combination R-PDT + ∝PD-1 (n=5 per group). Levels of IL-6 (A), albumin (B), globulins (C) were quantified. Serum levels of IL-1α (D), CXCL5 (E), and MIP-2 (F) were also investigated. Flow cytometry was performed to assess the frequency of NK1.1+ cells in the non-irradiated tumor (non-irrad Tumor) (G), spleen (H), and non-irradiated tumor draining lymph nodes (non-irrad tdLN) (I). For statistical analyses, a one-way ANOVA was performed, with a post-hoc Tukey test to differentiate significant differences between treatment groups. * denotes $p<0.05$, ** denotes $p<0.01$, *** denotes $p<0.001$, **** denotes $p < 0.0001$.

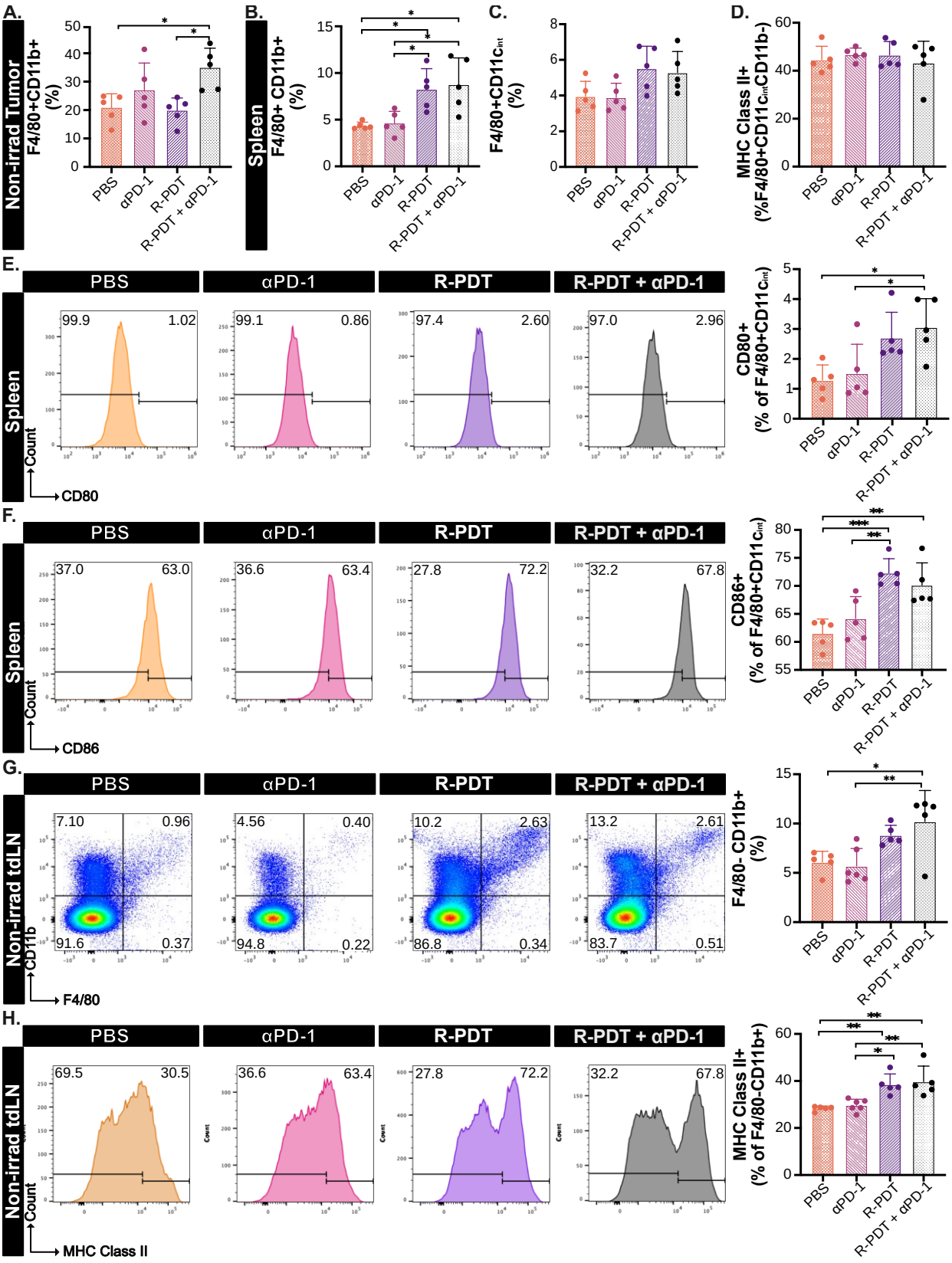
A.
Non-irrad Tumor F4/80+CD11b+ (%)
B.
Spleen F4/80+ CD11b+ (%)
C.
F4/80+CD11c$_{int}$ (%)
D.
MHC Class II+ (%F4/80+CD11c$_{int}$CD11b-)
PBS
αPD-1
R-PDT
R-PDT + αPD-1
E.
Spleen
99.9
1.02
99.1
0.86
97.4
2.60
97.0
2.96
Count
CD80
CD80+ (% of F4/80+CD11c$_{int}$)
F.
Spleen
37.0
63.0
36.6
63.4
27.8
72.2
32.2
67.8
CD86
CD86+ (% of F4/80+CD11c$_{int}$)
G.
Non-irrad tdLN
7.10
0.96
91.6
0.37
4.56
0.40
94.8
0.22
10.2
2.63
86.8
0.34
13.2
2.61
83.7
0.51
CD11b
F4/80
F4/80- CD11b+ (%)
H.
Non-irrad tdLN
69.5
30.5
36.6
63.4
27.8
72.2
32.2
67.8
MHC Class II
MHC Class II+ (% of F4/80-CD11b+)

Figure 4. Macrophage populations upregulate costimulatory molecules after repeated photodynamic therapy (R-PDT) and combination R-PDT + anti-PD-1 monoclonal antibody (∝PD-1) treatment. Flow cytometry was employed to quantify myeloid cell populations after mice were treated with phosphate buffered saline (PBS), ∝PD-1 (12 mg/kg), R-PDT (4 mg/kg PLP), or R-PDT + ∝PD-1 (12 mg/kg ∝-PD-1 and 4 mg/kg PLP; n=5 per group). F4/80+CD11b+ macrophages in the non-irradiated tumor (non-irrad tumor) (A) and spleen (B) are shown. F4/80+ $CD11c_{int}$ myeloid cells, some of which comprise red pulp macrophages in the spleen (C) and their corresponding levels of MHC class II expression (D) are displayed. Representative histograms of CD80 and CD86 expression on F4/80+$CD11c_{int}$ from one mouse per group and the group summary are shown in (E) and (F), respectively. In the non-irradiated tumor draining lymph nodes (non-irrad tdLN), populations of F4/80-CD11b+ myeloid cells after treatment are displayed in the representative flow plots and group summary in (G). MHC class II expression of F4/80-CD11b+ myeloid cells are shown in (H). For statistical analyses, a one-way ANOVA was performed, with a post-hoc Tukey test to differentiate significant differences between treatment groups. * denotes $p<0.05$, ** denotes $p<0.01$, *** denotes $p<0.001$, **** denotes $p<0.0001$.

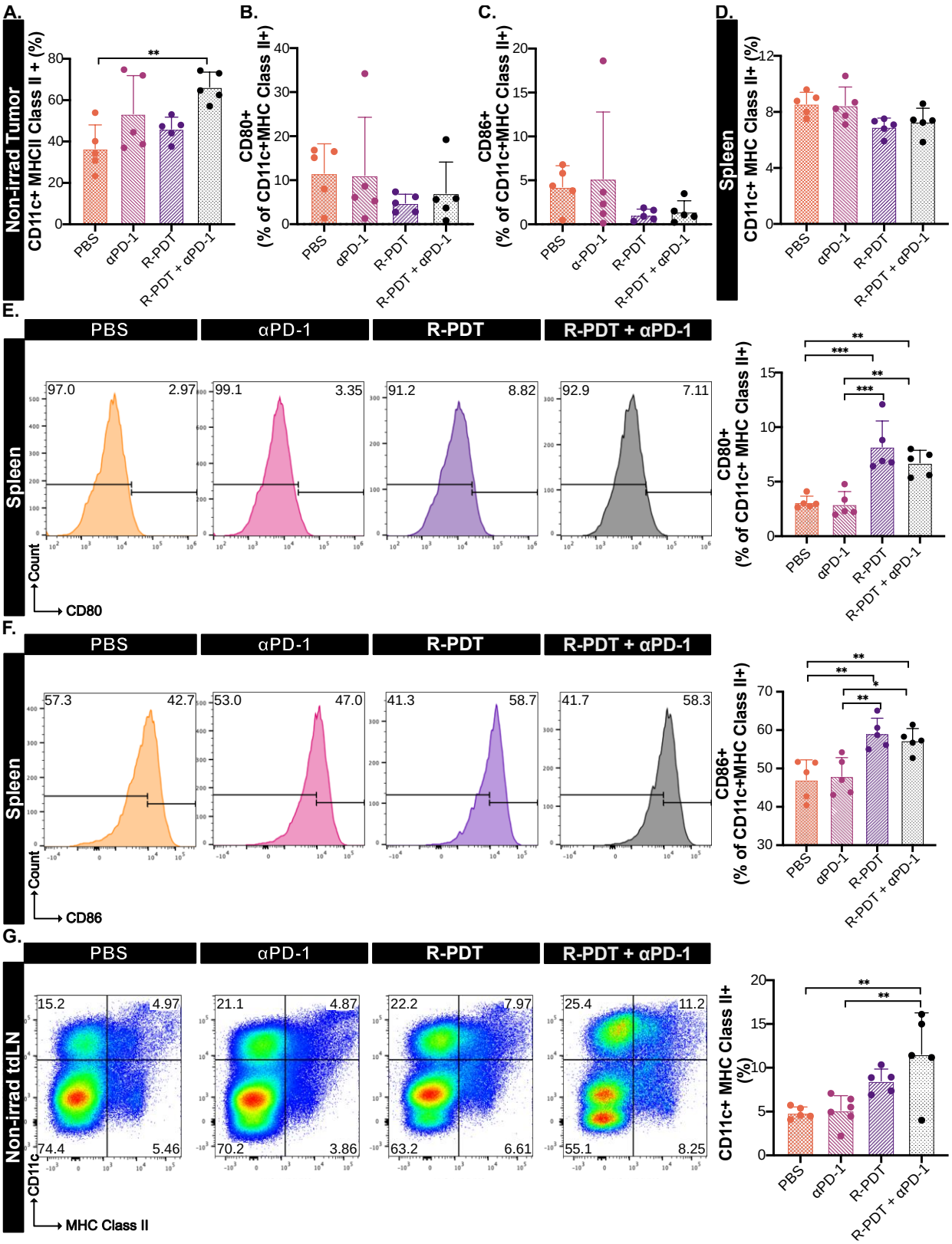

Figure 5. Dendritic cells upregulate costimulatory molecules after repeated photodynamic therapy (R-PDT) and combination R-PDT + anti-PD-1 monoclonal antibody (∝PD-1) treatment, indicative of T cell priming. To quantify dendritic cells in the non-irradiated tumor (non-irrad

tumor), spleen, and non-irradiated tumor draining lymph nodes (non-irrad tdLN), flow cytometry was performed on organs after dissection from mice treated with phosphate buffered saline (PBS), ∝PD-1 (12 mg/kg), R-PDT (4 mg/kg PLP), or R-PDT + ∝PD-1 (12 mg/kg ∝PD-1 and 4 mg/kg PLP; n=5 per group). CD11c+MHC class II+ dendritic cells from the non-irrad tumor are presented in (A), alongside their expression of costimulatory molecules, CD80 (B) and CD86 (C). Splenic CD11c+MHC class II+ dendritic cells are shown in (D). Representative histograms of CD80 and CD86 expression on splenic CD11c+MHC class II+ dendritic cells from one mouse per group and the group summary are shown in (E) and (F), respectively. In the non-irrad tdLN, populations of CD11c+MHC class II+ dendritic cells after treatment are displayed in the representative flow plots and group summary in (G). For statistical analyses, a one-way ANOVA was performed, with a post-hoc Tukey test to differentiate significant differences between treatment groups. * denotes $p<0.05$, ** denotes $p<0.01$, *** denotes $p<0.001$, **** denotes $p<0.0001$.

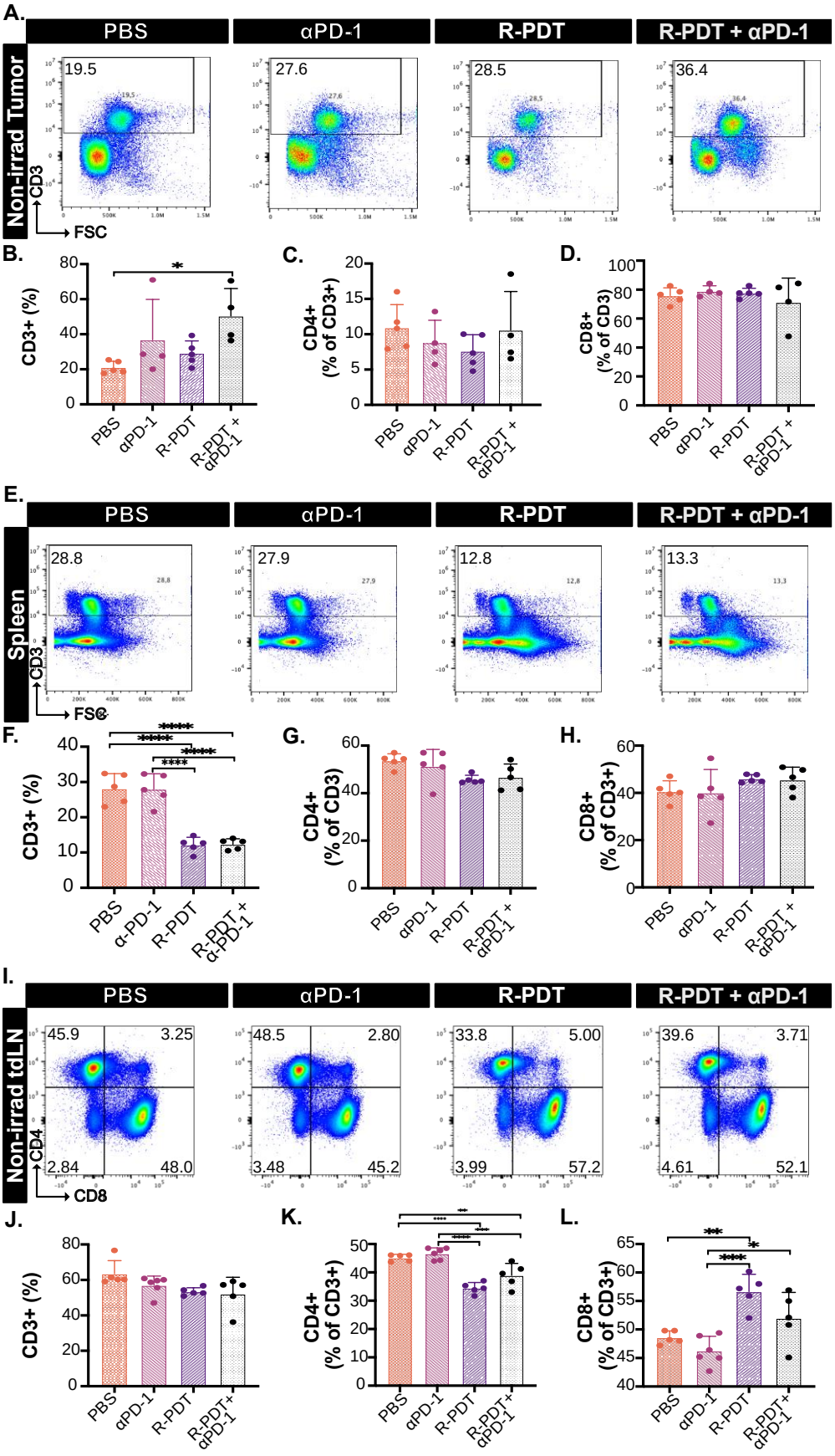
A.
PBS
αPD-1
R-PDT
R-PDT + αPD-1
Non-irrad Tumor
19.5
27.6
28.5
36.4
CD3
FSC
B.
CD3+ (%)
C.
CD4+ (% of CD3+)
D.
CD8+ (% of CD3)
PBS
αPD-1
R-PDT
R-PDT + αPD-1
E.
Spleen
28.8
27.9
12.8
13.3
F.
CD3+ (%)
G.
CD4+ (% of CD3)
H.
CD8+ (% of CD3+)
I.
Non-irrad tdLN
45.9
3.25
2.84
48.0
48.5
2.80
3.48
45.2
33.8
5.00
3.99
57.2
39.6
3.71
4.61
52.1
CD4
CD8
J.
CD3+ (%)
K.
CD4+ (% of CD3+)
L.
CD8+ (% of CD3+)
PBS
αPD-1
R-PDT
R-PDT+ αPD-1

Figure 6. CD3+ T cell populations are altered after repeated photodynamic therapy (R-PDT) and combination R-PDT + anti-PD-1 monoclonal antibody (∝PD-1) across the non-irradiated tumor (non-irrad tumor), spleen, and non-irradiated tumor draining lymph node (non-irrad tdLN). Flow cytometry was performed to quantify CD3+, CD4+, and CD8+ T-cell populations in mice treated with PBS, ∝PD-1 (12 mg/kg), R-PDT (4 mg/kg PLP), or R-PDT + ∝PD-1 (12 mg/kg ∝-PD-1 and 4 mg/kg PLP; n=5 per group). Representative dot plots of CD3+ T cells in the non-irrad tumor for mice with the different treatment groups and the group summary are shown in (A) and (B), respectively. CD4+ and CD8+ T cells in the non-irrad tumor are displayed in (C) and (D), respectively. For CD3+ T cells in the spleen, representative dot plots for the four treatment groups are shown in (E) and summarized for the group in (F). CD4+ and CD8+ T cells in the spleen are displayed in (G) and (H), respectively. Representative dot plots for CD4+ and CD8+ T cells in the non-irrad tdLN from mice receiving the different treatments are shown in (I). CD3+, CD4+, and CD8+ T cells from the non-irrad tdLN are summarized in (J), (K), and (L), respectively. For statistical analyses, a one-way ANOVA was performed, with a post-hoc Tukey test to differentiate significant differences between treatment groups. * denotes $p<0.05$, ** denotes $p<0.01$, *** denotes $p<0.001$, **** denotes $p < 0.0001$.

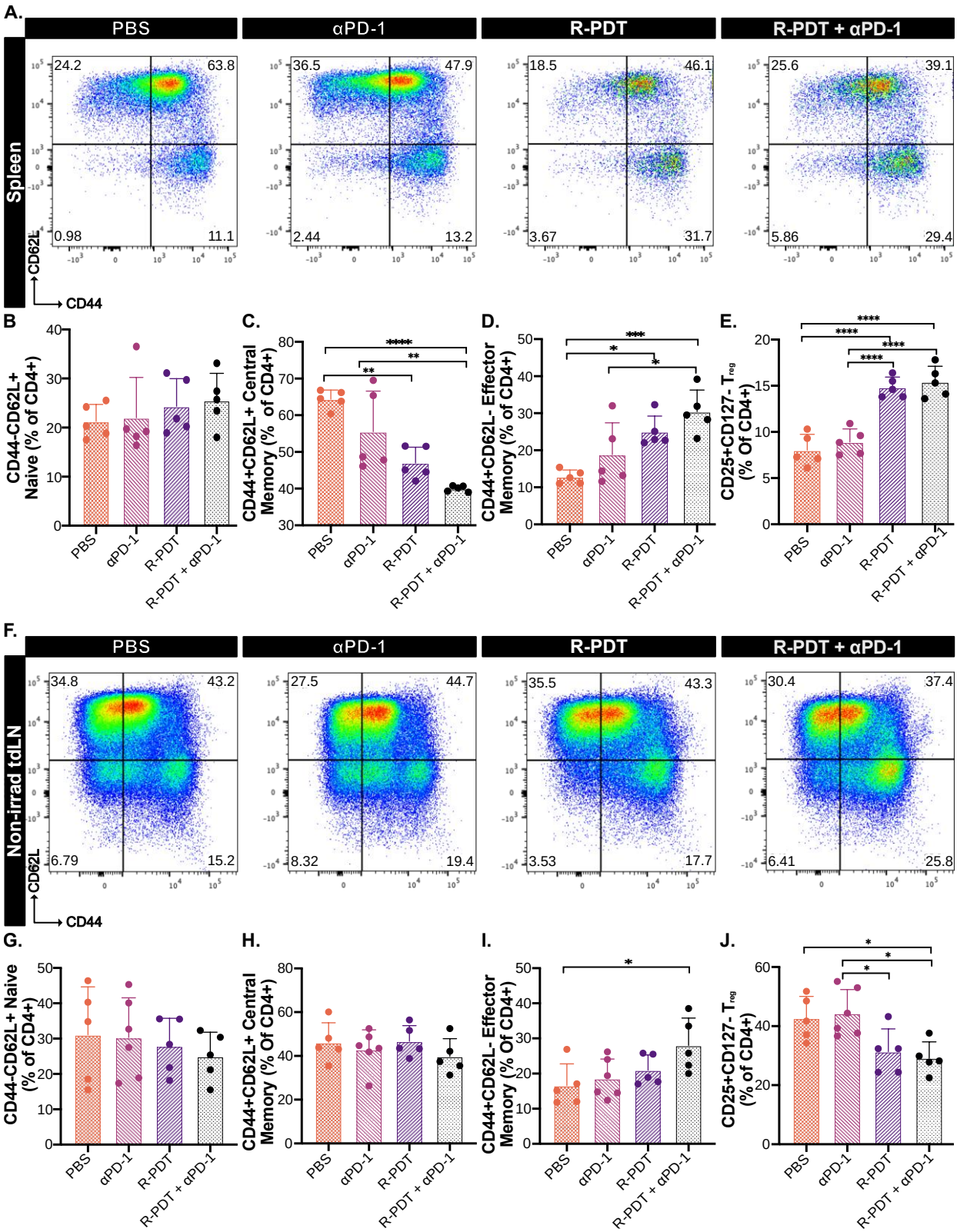

Figure 7. Repeated photodynamic therapy (R-PDT) and combination R-PDT + anti-PD-1 monoclonal antibody (∝PD-1) shift CD4+ T cell subsets in the spleen and non-irradiated tumor draining lymph nodes (non-irrad tdLN). To assess CD4+ T cell subsets, flow cytometry was

performed on the spleen and non-irrad tdLN from mice treated with either PBS, ∝PD-1 (12 mg/kg), R-PDT (4 mg/kg PLP), or R-PDT + ∝PD-1 (12 mg/kg ∝PD-1 and 4 mg/kg PLP; n=5 per group). For the spleen, representative dot plots of CD62L+ and CD44+ T cells, gated on CD3+ and CD4+ T cells, are displayed in (A). Splenic CD4+ CD44-CD62L+ naïve, CD44+CD62L+ central memory, and CD44+CD62L- effector memory T cells are quantified in (B), (C), and (D), respectively. For the non-irrad tdLN, representative dot plots of CD62L+ and CD44+ T cells, gated on CD3+ and CD4+ T cells, are displayed in (E). CD44-CD62L+ naïve, CD44+CD62L+ central memory, and CD44+CD62L- effector memory T cells are quantified in (F), (G), and (D=H), respectively. For statistical analyses, a one-way ANOVA was performed, with a post-hoc Tukey test to differentiate significant differences between treatment groups. * denotes $p<0.05$, ** denotes $p<0.01$, *** denotes $p<0.001$, **** denotes $p < 0.0001$.

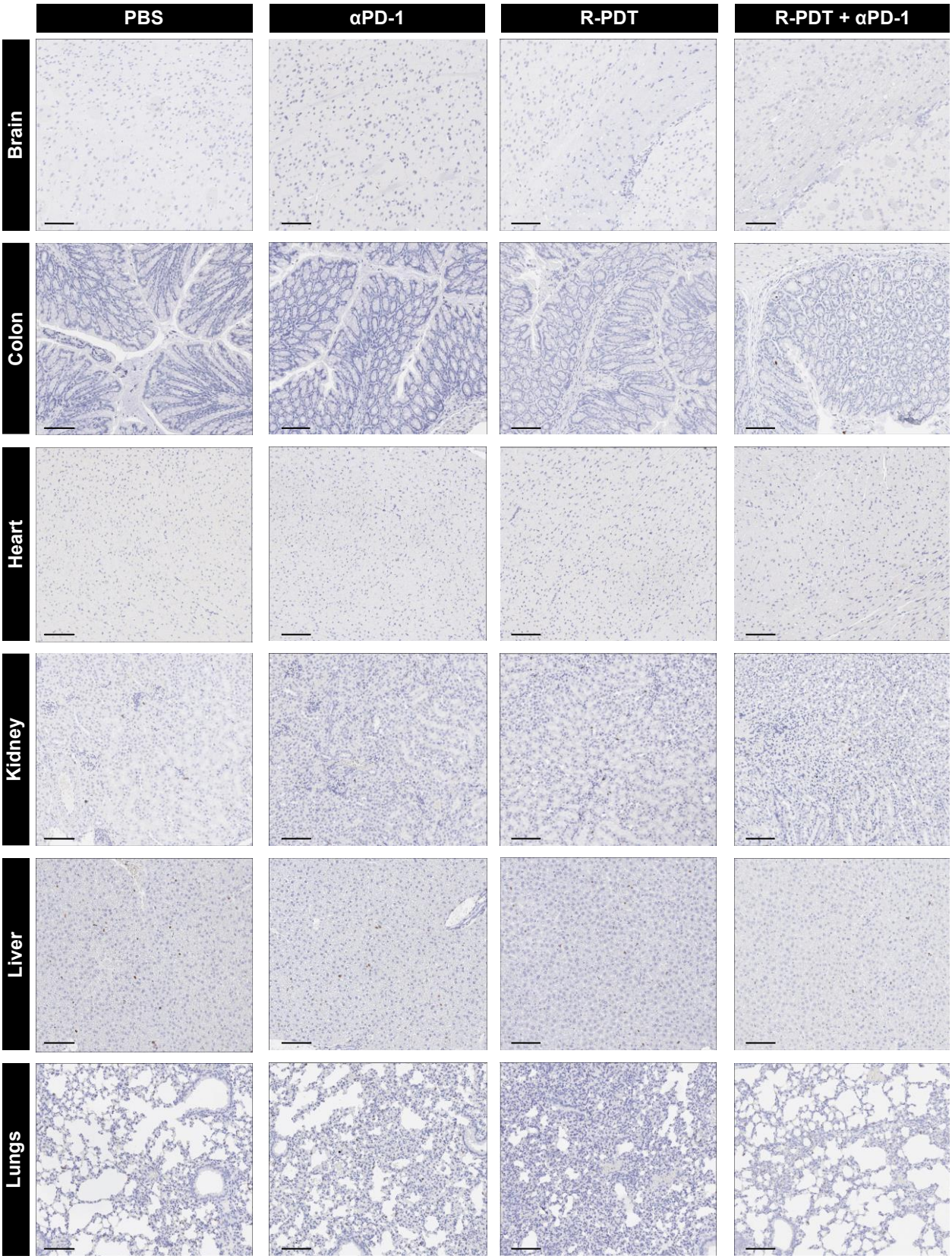

Figure 8. CD4+ T cell infiltration in major organs of mice did not differ after treatment with

repeated photodynamic therapy (R-PDT) and combination R-PDT + anti-PD-1 monoclonal antibody (∝PD-1) relative to saline-treated mice.
Mice were treated with phosphate buffered saline (PBS), ∝PD-1 (12 mg/kg), R-PDT (4 mg/kg PLP), or R-PDT + ∝PD-1 (12 mg/kg ∝PD-1 and 4 mg/kg PLP; n=5 per group). CD4+ staining was performed on the brain, colon, heart, kidney, liver, and lungs after treatment. Representative images for these organs are shown for each treatment group. Scale bars represent 100 μm.

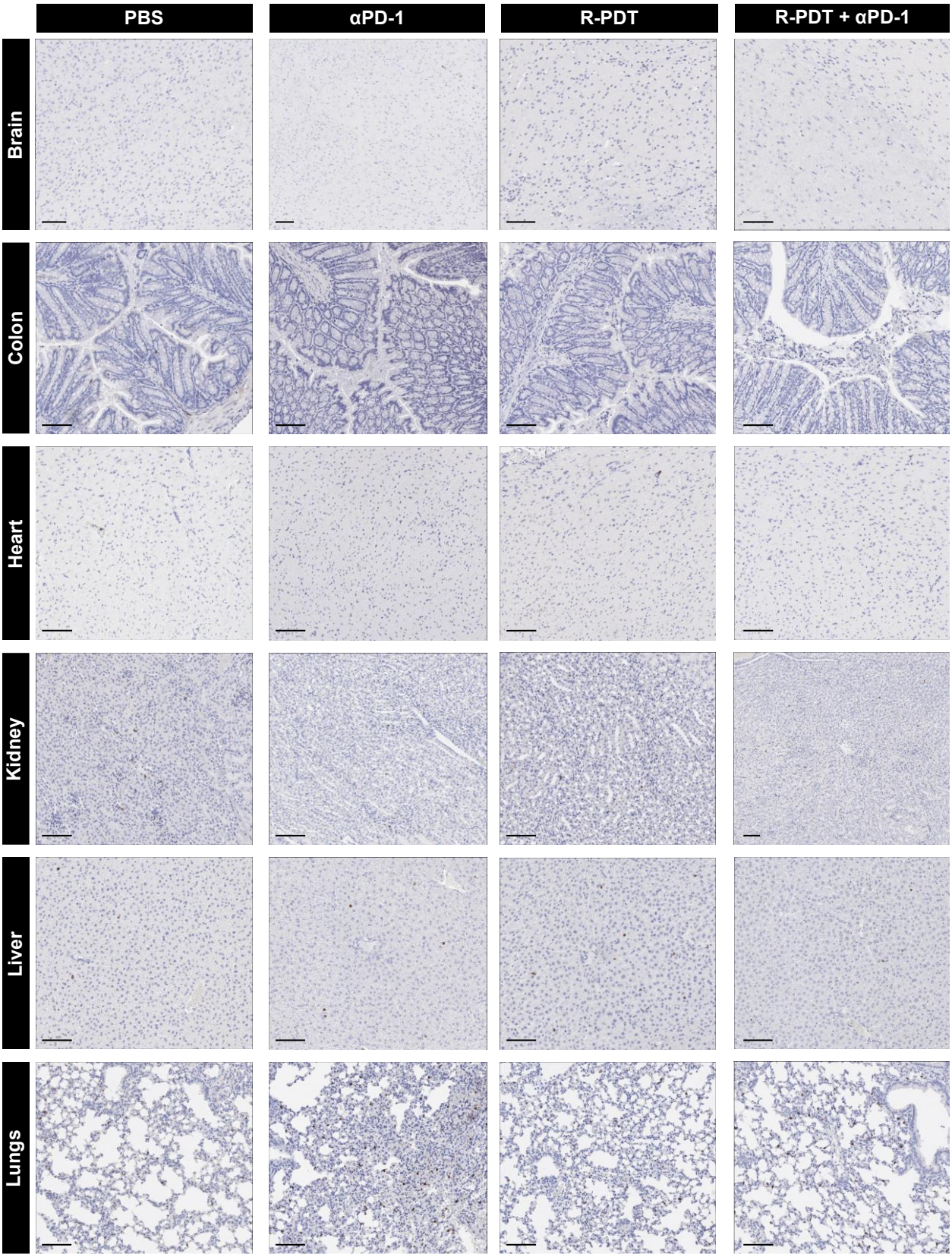

Figure 9. Similar CD8+ T cell infiltration in major organs of mice after treatment with repeated photodynamic therapy (R-PDT) and combination R-PDT + anti-PD-1 monoclonal antibody

(∝PD-1), relative to treatment with saline. Mice were treated with phosphate buffered saline (PBS), ∝PD-1 (12 mg/kg), R-PDT (4 mg/kg PLP), or R-PDT + ∝PD-1 (12 mg/kg ∝PD-1 and 4 mg/kg PLP; n=5 per group). After treatment, the brain, colon, heart, kidney, liver, and lungs were excised and processed for histology. Representative images for these organs stained for CD8 are shown for each treatment group. Scale bars represent 100 μm.

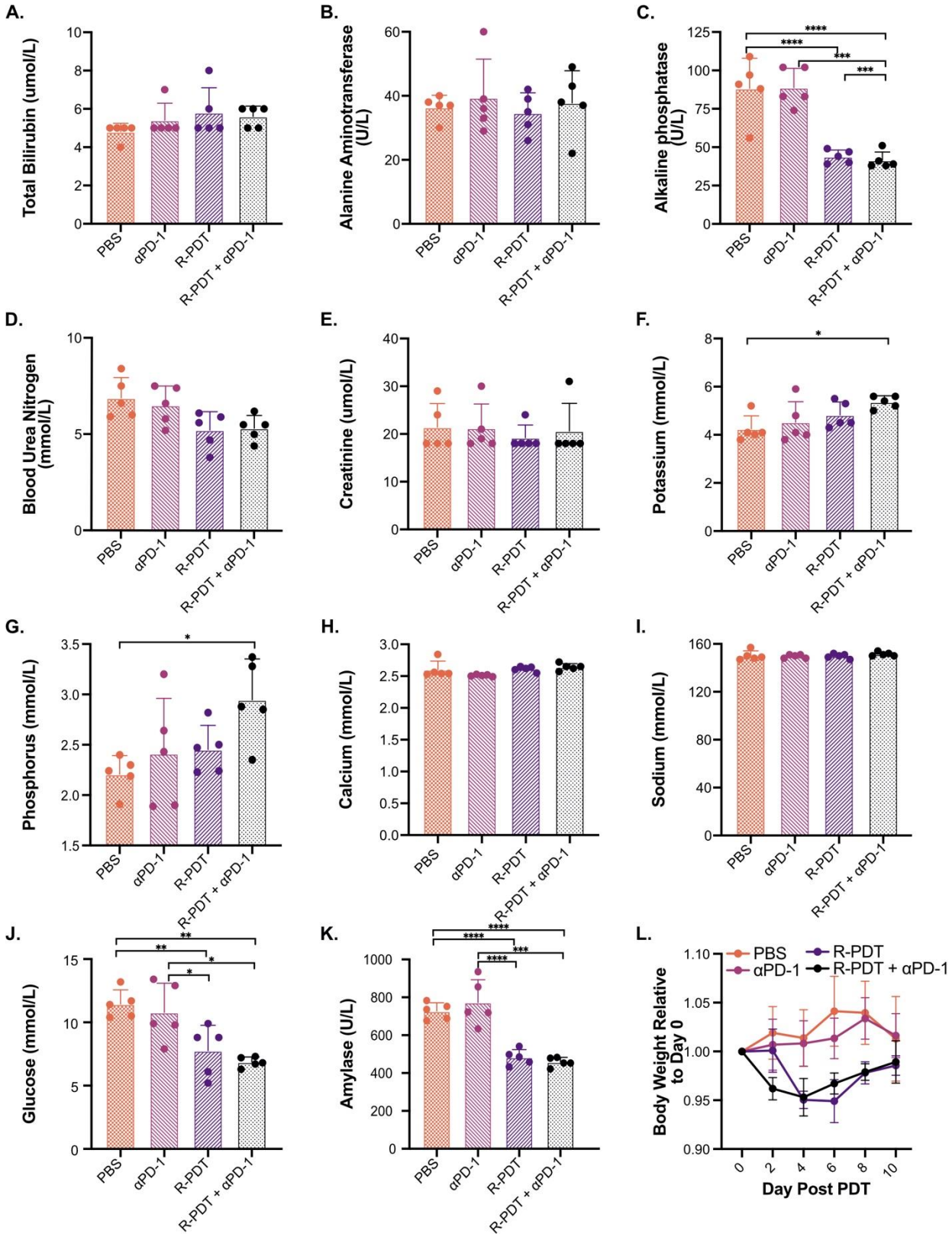

Figure 10. Minor alterations to liver and kidney function after repeated photodynamic therapy (R-PDT) and combination R-PDT + anti-PD-1 monoclonal antibody (∝PD-1). Serum was obtained from mice after treatment with either phosphate buffered saline (PBS), ∝PD-1 (12

mg/kg), R-PDT (4 mg/kg PLP), or R-PDT + ∝PD-1 (12 mg/kg ∝PD-1 and 4 mg/kg PLP; n=5 per group). Liver enzymes, including total bilirubin (A), alanine aminotransferase (B), and alkaline phosphatase (C) were quantified. Indicators of kidney function, such as blood urea nitrogen (D), creatinine (E), potassium (F), calcium (G), sodium (H), and phosphorus (I) were assessed. Levels of glucose (J) and amylase (K) were also investigated. Body weights of mice were measured (L). For statistical analyses, a one-way ANOVA was performed, with a post-hoc Tukey test to differentiate significant differences between treatment groups. * denotes $p<0.05$, ** denotes $p<0.01$, *** denotes $p<0.001$, **** denotes $p < 0.0001$.

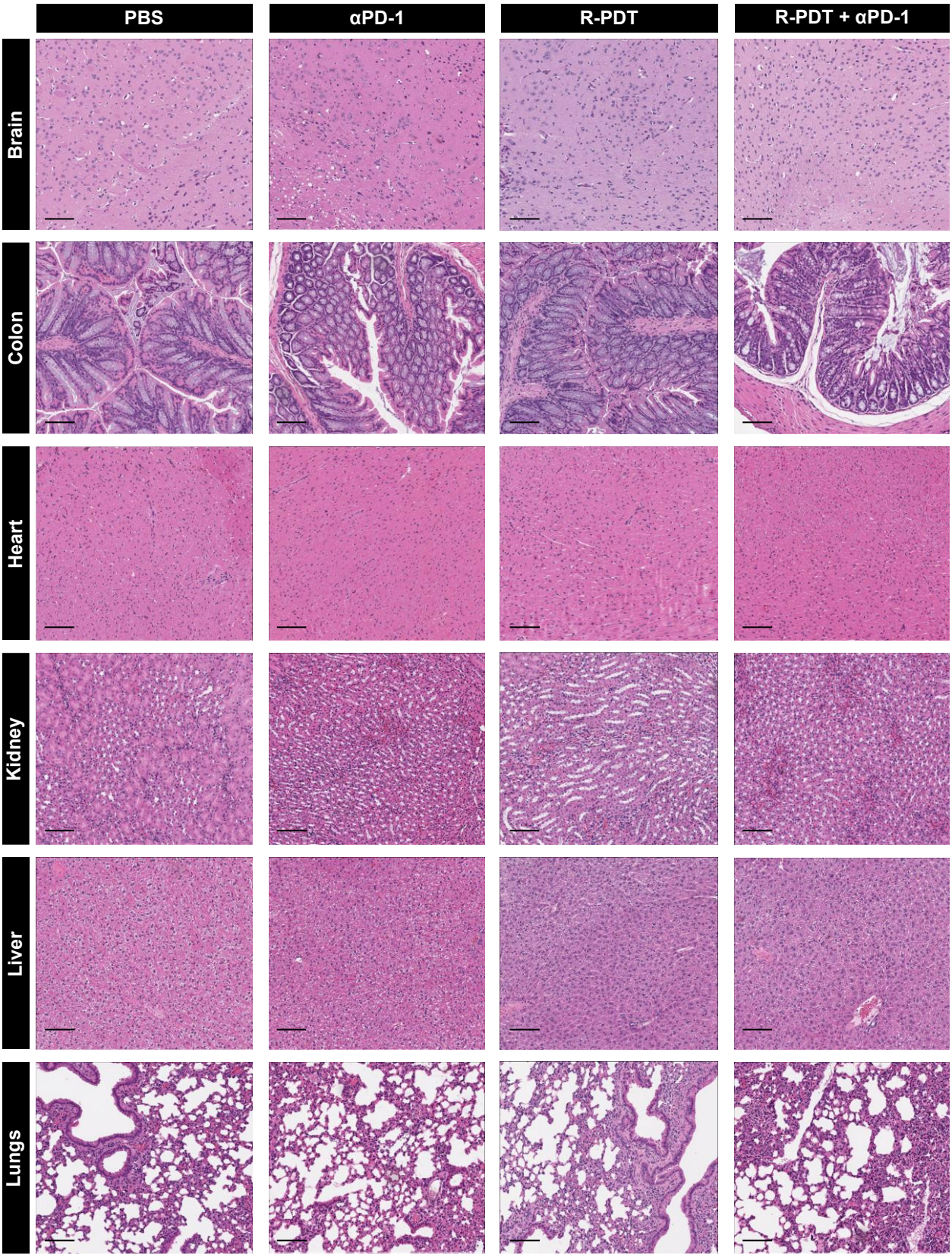

Figure 11. Hematoxylin and eosin staining of the brain, colon, heart, kidney, liver, and lungs of mice after treatment with phosphate buffered saline (PBS), anti-PD-1 monoclonal antibody

(∝PD-1), repeated photodynamic therapy (R-PDT), or combination R-PDT + ∝PD-1. Dual subcutaneous AE17-OVA+ tumor bearing mice received PBS, αPD-1 (12 mg/kg), PDT (PLP at 4 mg/kg), or combination αPD-1 antibody (12 mg/kg) and R-PDT (PLP at 4 mg/kg) four times. Scale bars represent 100 μm.

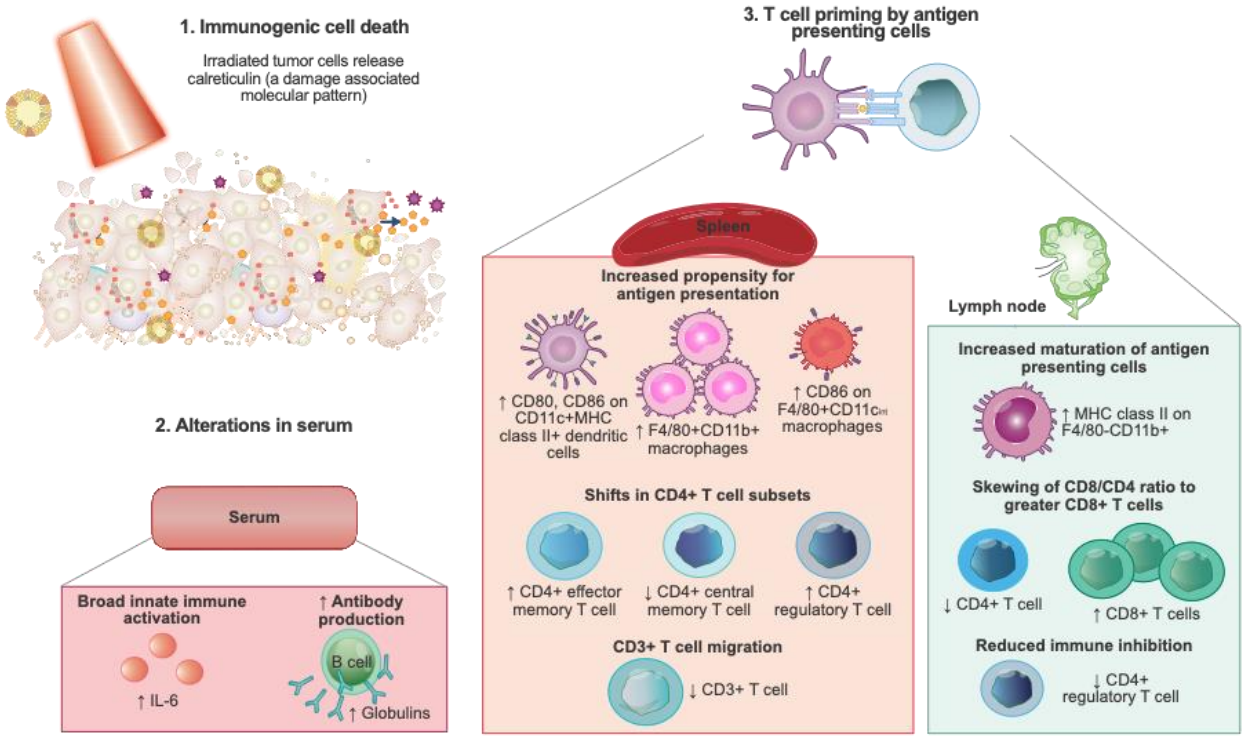

Figure 12. Overview of the immune crosstalk after repeated photodynamic therapy (R-PDT), which mediates a delay in distal, non-irradiated tumor growth.

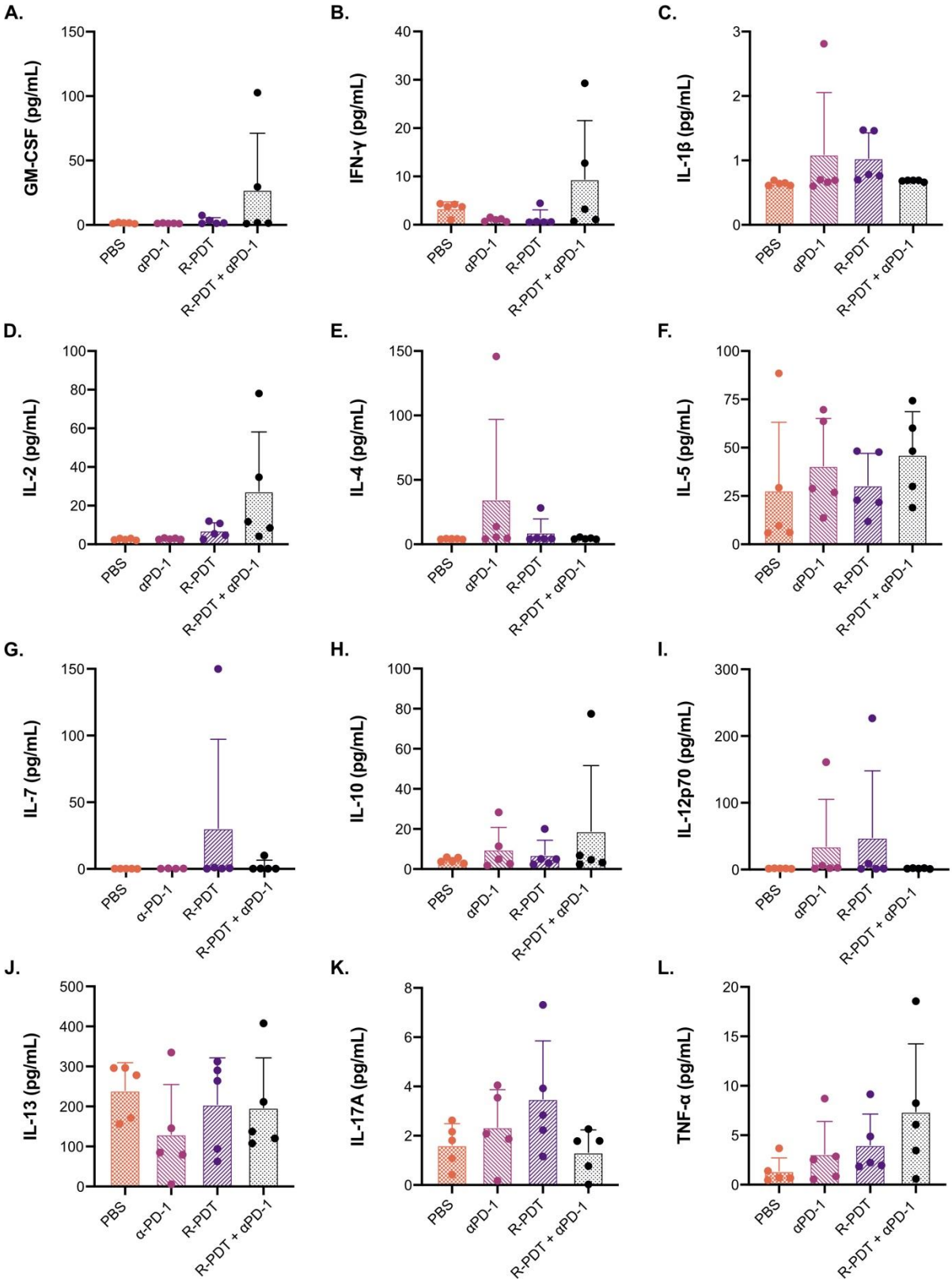

Supplementary Figure 1. Multiple serum cytokines were similar between treatment groups. Mice were treated with phosphate buffered saline (PBS), anti-PD-1 monoclonal antibody (∝PD-1; 12 mg/kg), repeated photodynamic therapy (R-PDT; 4 mg/kg PLP), or combination R-PDT + ∝PD-

1 (12 mg/kg ∝PD-1 and 4 mg/kg PLP; n=5 per group). Serum was collected and cytokines were assessed via fluorescence multiplexing. Various cytokines, such as GM-CSF (A), IFN-g (B), IL-1b (C), IL-2 (D), IL-4 (E), IL-5 (F), IL-7 (G), IL-10 (H), IL-12p70 (I), IL-13 (J), IL-17A (K), and TNF-a (L), were quantified.

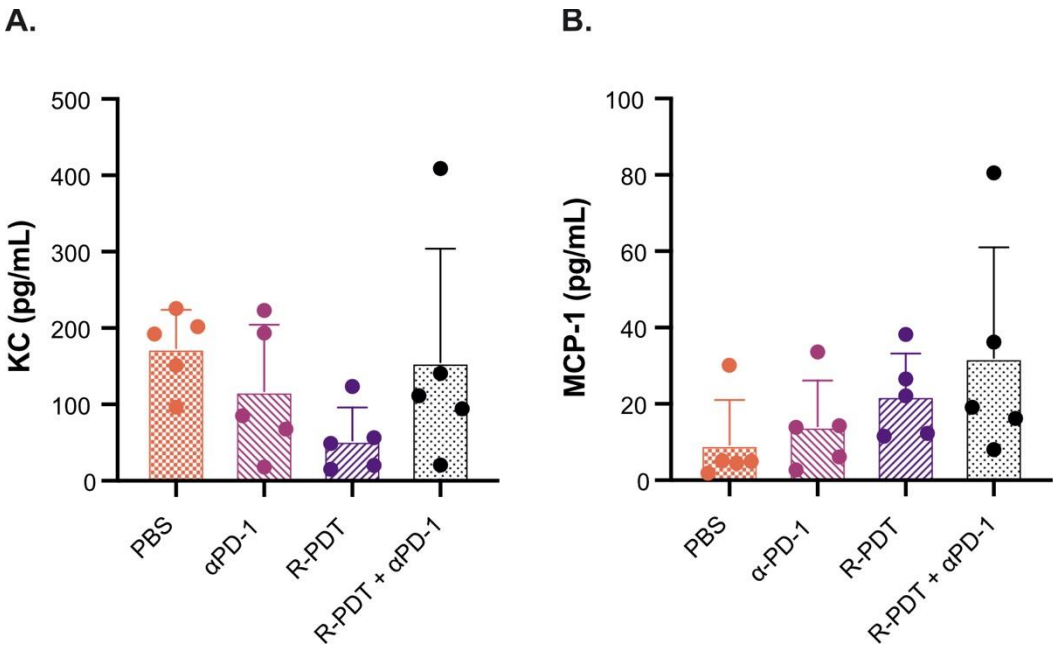

Supplementary Figure 2. Serum chemokines, KC and MCP-1, did not differ after repeated photodynamic therapy (R-PDT) and combination R-PDT + ∝PD-1. Mice were treated with phosphate buffered saline (PBS), anti-PD-1 monoclonal antibody (∝PD-1; 12 mg/kg), repeated photodynamic therapy (R-PDT; 4 mg/kg PLP), or combination R-PDT + ∝PD-1 (12 mg/kg ∝PD-1 and 4 mg/kg PLP; n=5 per group). Serum was collected and chemokines were assessed via fluorescence multiplexing.

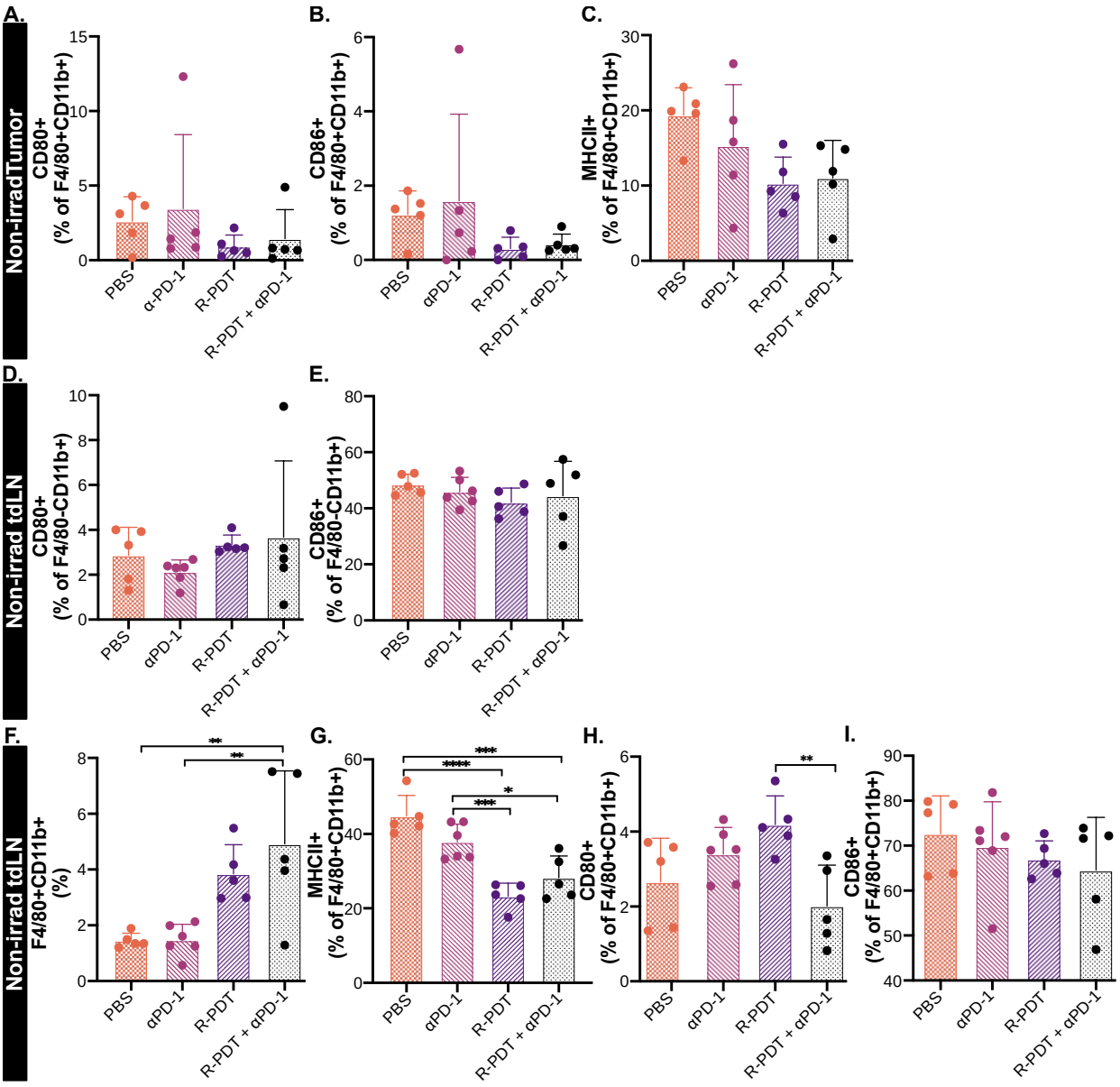

Supplementary Figure 3. Maturation and costimulatory markers on myeloid cells in the non-irradiated tumor and non-irradiated tumor-draining lymph nodes. Flow cytometry was used to assess the upregulation of MHC class II, CD80, and CD86 molecules on myeloid cells in the non-irradiated tumor (non-irrad tumor) and non-irradiated tumor-draining lymph nodes (non-irrad tdLN), after mice were treated with phosphate buffered saline (PBS), anti-PD-1 monoclonal antibody (∝PD-1; 12 mg/kg), repeated photodynamic therapy (R-PDT; 4 mg/kg PLP), or R-PDT + ∝PD-1 (12 mg/kg ∝-PD-1 and 4 mg/kg PLP; n=5 per group). For F4/80+CD11b+ macrophages in the tumor, expression of MHC class II molecules, CD80, and CD86 molecules are shown in (A), (B), and (C), respectively. Levels of CD80 and CD86 for F4/80-CD11b+ myeloid cells in the non-irrad tdLN are summarized in (D) and (E), respectively. The expression of MHC class II, CD80, and CD86 molecules on nodal F4/80+CD11b+ myeloid cells are displayed in (F), (G), and (H), respectively.

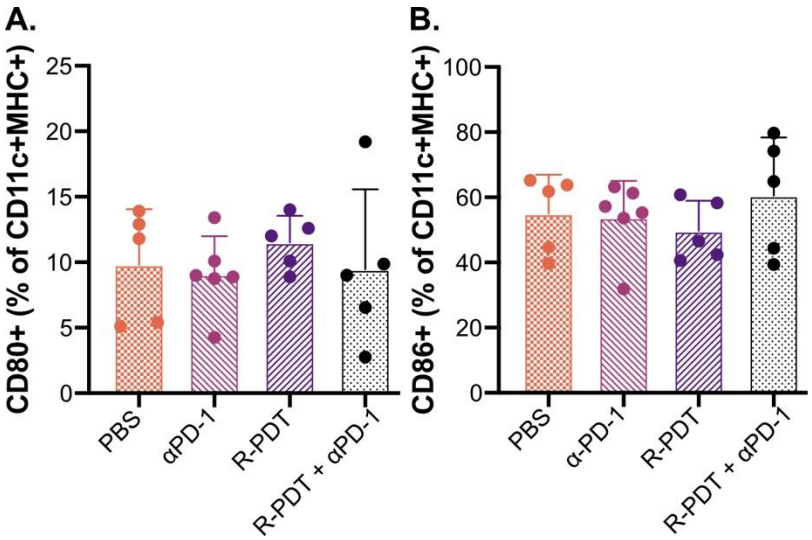

Supplementary Figure 4. Expression of costimulatory molecules on dendritic cells in the non-irradiated tumor-draining lymph nodes are similar between treatment groups. Flow cytometry was used to assess the upregulation of CD80 and CD86 molecules on dendritic cells in non-irradiated tumor-draining lymph nodes, after mice were treated with phosphate buffered saline (PBS), anti-PD-1 monoclonal antibody (∝PD-1; 12 mg/kg), repeated photodynamic therapy (R-PDT; 4 mg/kg PLP), or R-PDT + ∝PD-1 (12 mg/kg ∝-PD-1 and 4 mg/kg PLP; n=5 per group). Expression of CD80 and CD86 molecules are shown in (A) and (B), respectively.

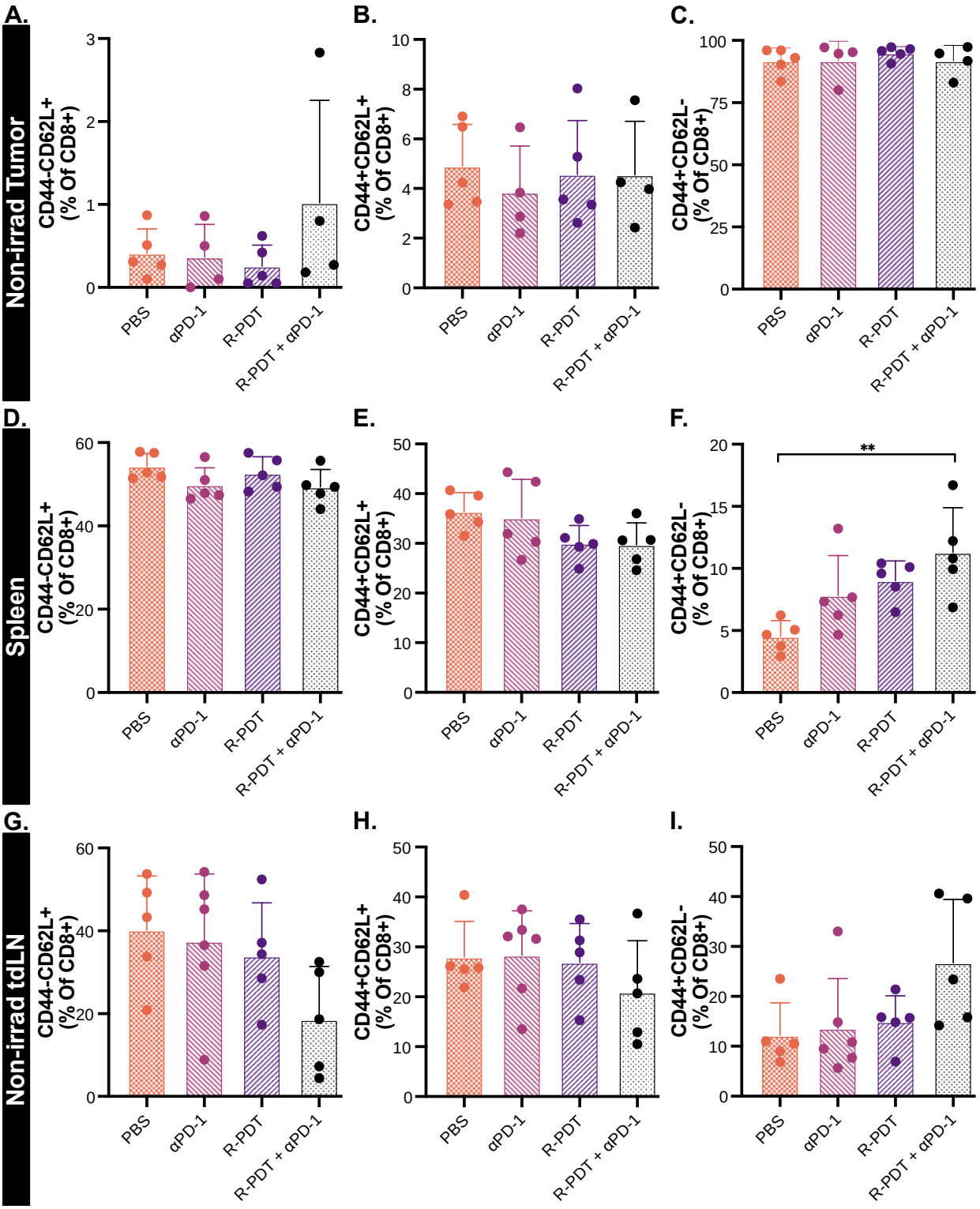

Supplementary Figure 5. CD8+ T cell subsets in the non-irradiated tumor, spleen, and non-irradiated tumor-draining lymph nodes are largely similar across treatment groups. To assess CD8+ T cell subsets, flow cytometry was performed on the non-irradiated tumor (non-irrad tumor), spleen, and non-irradiated tumor draining lymph nodes (non-irrad tdLN) of mice treated with either phosphate buffered saline (PBS), anti-PD-1 monoclonal antibody (∝PD-1; 12

mg/kg), repeated photodynamic therapy (R-PDT; 4 mg/kg PLP), or R-PDT + ∝PD-1 (12 mg/kg ∝-PD-1 and 4 mg/kg PLP; n=4-5 per group). CD8+ CD44-CD62L+ naïve, CD44+CD62L+ central memory, and CD44+CD62L- effector memory T cells from the non-irrad tumor are quantified in (A), (B), and (C), respectively. Splenic CD44-CD62L+ naïve, CD44+CD62L+ central memory, and CD44+CD62L- effector memory T cells are displayed in (D), (E), and (F), respectively. For the non-irrad tdLN, CD44-CD62L+ naïve, CD44+CD62L+ central memory, and CD44+CD62L- effector memory T cells are displayed in (G), (H), and (I), respectively.

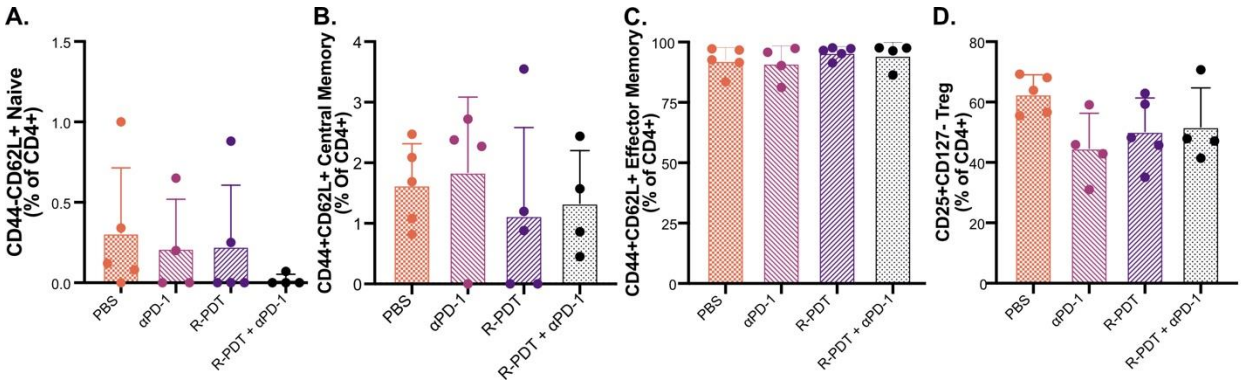

Supplementary Figure 6. CD4+ T cell subsets in the tumor are similar between treatment groups. To assess CD4+ T cell subsets, flow cytometry was performed on the non-irradiated tumor of mice treated with either phosphate buffered saline (PBS), anti-PD-1 monoclonal antibody (∝PD-1; 12 mg/kg), repeated photodynamic therapy (R-PDT; 4 mg/kg PLP), or R-PDT + ∝PD-1 (12 mg/kg ∝-PD-1 and 4 mg/kg PLP; n=4-5 per group). CD4+ CD44-CD62L+ naïve, CD44+CD62L+ central memory, CD44+CD62L- effector memory T cells, and CD25+CD127 T_{regs} are quantified in (A), (B), (C), and (D), respectively.